Agricultural and Forest Meteorology 265 (2019) 30–47

Contents lists available at ScienceDirect

Agricultural and Forest Meteorology

journal homepage: www.elsevier.com/locate/agrformet

The breathing of the Andean highlands: Net ecosystem exchange and evapotranspiration over the páramo of southern Ecuador

Galo Carrillo-Rojas[a,b,c,*], Brenner Silva[a], Rütger Rollenbeck[a], Rolando Célleri[b,c], Jörg Bendix[a]

[a] Laboratory for Climatology and Remote Sensing, Faculty of Geography, Philipps-Universität Marburg, Deutschhausstr. 12, Marburg 35032, Germany
[b] Departamento de Recursos Hídricos y Ciencias Ambientales, Universidad de Cuenca, Campus Balzay, Cuenca 010207, Ecuador
[c] Facultad de Ciencias Químicas, and Facultad de Ingeniería, Universidad de Cuenca, Av. 12 de Abril y A. Cueva, Cuenca 010203, Ecuador

ARTICLE INFO

Keywords:
Tropical Andes
Ecuador
Páramo
Eddy covariance
Carbon
Evapotranspiration

ABSTRACT

Atmospheric carbon (CO_2) exchange, evapotranspiration (ET) processes, and their interactions with climatic drivers across tropical alpine grasslands are poorly understood. This lack of understanding is particularly evident for the páramo, the highest vegetated frontier in the northern Andes, the main source of water for inter-Andean cities, and a large carbon storage area. Studies of CO_2 and ET fluxes via the standard Eddy Covariance (EC) technique have never been applied to this region, limiting the understanding of diurnal / nocturnal exchanges and budget estimations. In this paper, we report the first EC analysis conducted on the Andean páramo (3765 m a.s.l.); this analysis measured CO_2, ET, and micrometeorological variables over two years (2016–2018) to understand their interactions with climatic / biophysical controls. The páramo was found to be a source of CO_2 and exhibited a net positive exchange (mean = +99 ± 30 gC m^{-2} per year). The light-responses of net CO_2 exchange and the primary productivity were correlated and model-parameterized. Evapotranspiration was 635 ± 9 mm per year (51% of the annual rainfall total), and we obtained crop coefficients for the dominant vegetation (Tussock grass) based on reference-ET models FAO56 and ASCE-ERWI (0.90 and 0.78, respectively). We also compared our results to those from other high-altitude (alpine) and high-latitude grasslands (tundra). Finally, we demonstrate that our measurement period is representative of the páramo's longer-term climate dynamics. Our investigation contributes to the body of knowledge on the land surface-atmosphere processes of the tropical Andes and supports decision-making about ecosystem services management and the preservation of this vulnerable biome.

1. Introduction

The tropical Andes leads the list of worldwide biodiversity hotspots (Myers et al., 2000). Approximately 6.7% of the globe's endemic plants and 5.7% of the world's vertebrate species are observed along the mountain gradient that extends to a vast alpine ecosystem between 3200 (subpáramo) and 4500 m a.s.l. (superpáramo or subnival) (Llambí et al., 2012). This neotropical biome covers large areas of Colombia (19,330 km^2), Ecuador (13,372 km^2), Venezuela (2660 km^2), Perú (462 km^2) and Central America (Costa Rica 150 km^2 and Panama 20 km^2) (Hofstede et al., 2014). The páramo extends across 7% of the Ecuadorian territory (Beltrán et al., 2009; Josse et al., 2009) and is highly biodiverse (Mena-Vásconez and Hofstede, 2006). Unfortunately, less than 40% of the area is formally protected (Cuesta and De Bièvre, 2008). The climate, soils and dominant vegetation (tussock grasses) of the area significantly affect water regulations and supplies for the heavily populated inter-Andean valleys (Buytaert et al., 2006a; Célleri and Feyen, 2009; Mosquera et al., 2015). Moreover, they form a massive organic carbon (C) pool (Bertzky et al., 2010; Farley et al., 2004; Hribljan et al., 2016). Unfortunately, the fragile ecosystem is clearly exposed to the negative effects of climate and land-use change (Harden et al., 2013; Vuille et al., 2003). Water vapor and carbon dioxide (CO_2) dynamics at regional and landscape scales are crucial elements in determining the aforementioned effects on this pristine environment (Herzog et al., 2011; Pepin et al., 2015). Thus, an understanding of the C assimilation and carbon / water relationships in the páramo is needed owing to its ecohydrological importance (Aparecido et al., 2018), as is the case for other mountainous tundra ecosystems. Unfortunately, land-atmosphere gas exchange processes of natural grasslands in the tropics remain unexplored (Fisher et al., 2009; Grace et al., 2006), especially those of the highlands, because relevant instrumentation for these remote areas is lacking (Pepin et al., 2015).

* Corresponding author at: Universidad de Cuenca - Campus Balzay, Av. V.M. Albornoz y de los Cerezos, Cuenca 010207, Ecuador.
E-mail address: galo.carrillo@ucuenca.edu.ec (G. Carrillo-Rojas).

https://doi.org/10.1016/j.agrformet.2018.11.006
Received 16 March 2018; Received in revised form 24 October 2018; Accepted 5 November 2018
Available online 15 November 2018

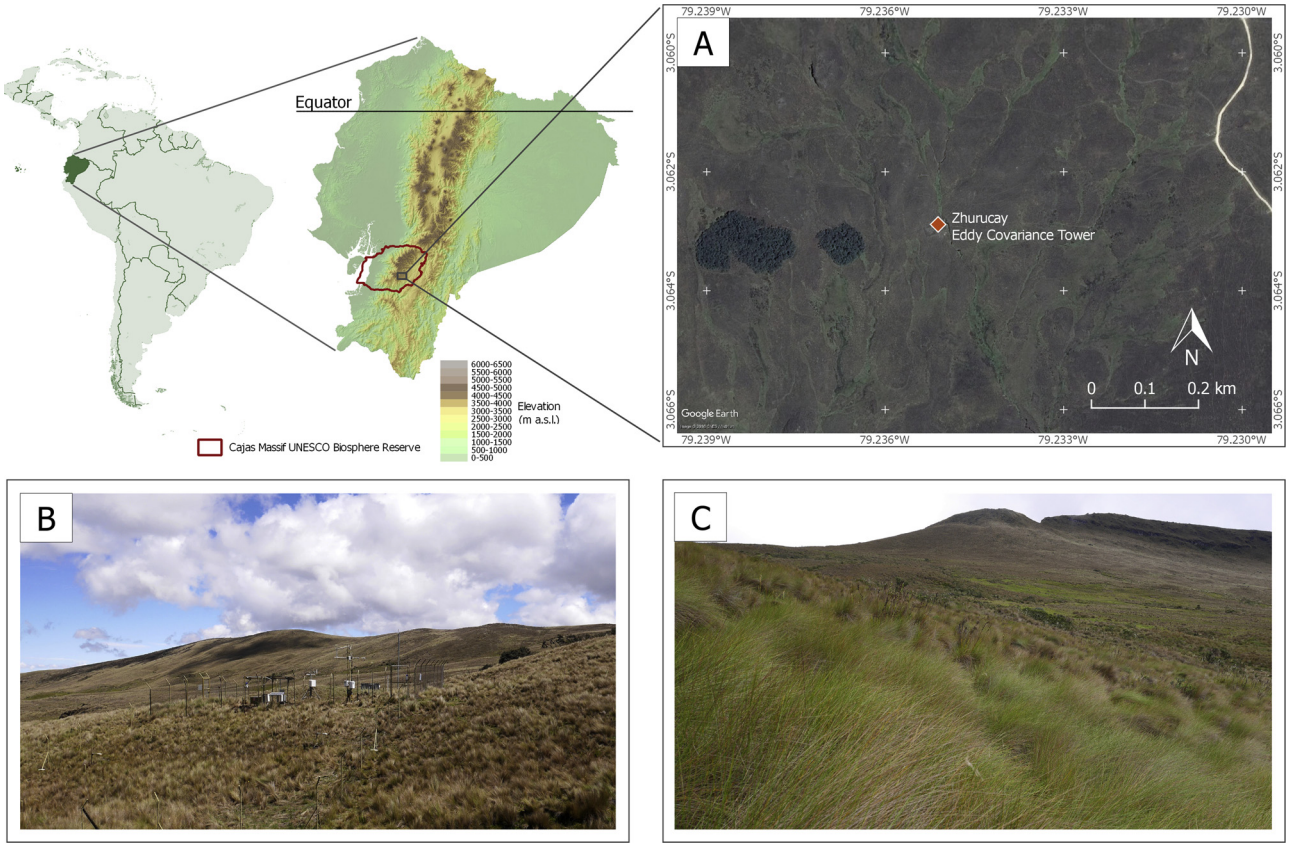

Fig. 1. Study Area: A) Satellite image of the location of the páramo ecosystem (Google Earth Pro, 2016), B) Landscape image of the Zhurucay Ecohydrological Observatory and the EC tower, and C) View of the main biome in the fetch (tussock grasslands).

The eddy covariance method (EC) has been proven to be a reliable technique for measuring gas and energy exchanges between land masses and the atmosphere across natural and disturbed areas (Baldocchi et al., 2001; Baldocchi, 2003; Burba, 2013; Munger et al., 2012). As a consequence, the EC method has been applied in over 562 active EC flux towers in the FLUXNET consortium, which covers diverse biomes (Baldocchi et al., 2001). However, EC implementation represents a challenge when nonideal conditions are present (Baldocchi, 2003); such nonideal conditions include complex terrain, in which uncertainties are related to nighttime advection effects (Galvagno et al., 2017; Novick et al., 2014) and to the incoming / outgoing energy observations that are affected by the underlying sloped surface (Wohlfahrt et al., 2016). Although its application to mountainous terrain has limitations, the EC technique allows one to obtain reliable energy, CO_2, and water vapor estimates when specific topographical corrections (Hiller et al., 2008), source analyses and data filtering (e.g., footprint modeling, low-turbulence fluxes removal) (Kljun et al., 2015; Rannik et al., 2012) and validation approaches (e.g., energy balance closure) (Foken, 2008; Leuning et al., 2012) are properly conducted. On this basis, two major EC-derived quantities are the most important for the analysis of the C and water balance of land surfaces: (i) the Net Ecosystem Exchange (NEE) and (ii) the Actual Evapotranspiration (ETa).

First, the NEE, which is the net CO_2 flux from the ecosystem to the atmosphere (CO_2 release = +NEE, and CO_2 uptake = –NEE), can be partitioned into Gross Primary Productivity (GPP) and Ecosystem Respiration (Reco) (Lasslop et al., 2010; Reichstein et al., 2005), which provide reliable insights into CO_2 assimilation / respiration processes. While GPP is considered to be the quantitatively most important global CO_2 flux (12 ± 8 PgC year^{-1}) (Beer et al., 2010), modeled or instrument-derived GPP estimates are rarely reported for the páramo. Limited data for this biome have been obtained only via the static flux chamber method (McKnight et al., 2017; Sánchez et al., 2017), empirically via the aboveground-biomass estimation (Ramsay and Oxley, 2001), or by computational simulations (i.e., via biogeochemical-physiological models such as BIOME-BCG) (Minaya, 2016; Minaya et al., 2016). In spite of their limitations (Damm et al., 2010; Heinsch et al., 2006), remote sensing-based GPP estimations (i.e., MODIS GPP product (Running et al., 2004)) have not been tested or validated for the páramo. Hence, in situ evaluations of NEE and GPP and their responses to light, humidity and temperature are central to a proper understanding of ecosystem productivity under cloudy, cold and humid conditions in tropical páramos.

Second, the ETa, a functional indicator of water stress affecting native tussock grasses, is another understudied variable of these mountain grasslands (Carrillo-Rojas et al., 2016). ETa is a key component of the hydrological cycle and therefore critical for water balance analyses (Buytaert et al., 2006c; Célleri and Feyen, 2009) and for studies of land-cover change in these locations (Crespo et al., 2010). Consequently, a thorough understanding of the relationships between primary productivity and micrometeorological conditions including ETa and the crop coefficients (Kc), used to convert reference evapotranspiration (ETr) to ETa, can lead to a better understanding of model-based estimations, which are generally not parameterized to the ecosystem. Neither indicators (NEE and ETa) has been well-studied in the Andean páramo.

In this paper, we present a pioneering EC-based investigation conducted in this relevant Andean ecosystem by describing: (i) the energy, CO_2 and water vapor exchange processes for a Neotropical site in southern Ecuador; (ii) the dependency of CO_2 uptake and release processes on soil temperature, humidity and light availability, (iii) the interpretation of the shorter-term results in the context of the longer-term climate drivers, particularly drought / water excess scenarios; and finally, (iv) the relationships between the observed ETa and the modeled ETr, which help determine the Kc of tussock grass via water vapor

detection (the EC technique).

2. Materials and methods

2.1. Study site characteristics

The study site is located in the Zhurucay Ecohydrological Observatory (FLUXNET EC-APr), which is positioned in the headwaters of a 7.53 km^2 catchment in southern Ecuador at 3765 m a.s.l. (the Northern Andean Páramo Ecoregion, according to Olson et al. (2001)). Hydrological, geochemical and landscape characteristics of the observatory have been extensively discussed in several studies (Córdova et al., 2015; Correa et al., 2017, 2016, Mosquera et al., 2016a, 2016b, 2015; Ochoa-Sánchez et al., 2018; Padrón et al., 2015; Quichimbo et al., 2012). Fig. 1 shows the study location, a satellite view of the site, and the landscape features surrounding the observatory.

The area studied plays a crucial role as a headwater basin within the Cajas Massif, a UNESCO World Biosphere Reserve (9766 km^2); more than 838,000 inhabitants in the inter-Andean and lowland valleys benefit from its water supply (Célleri and Feyen, 2009; UNESCO, 2013). The geology of the area belongs to the Quimsacocha and Turi formations (Mosquera et al., 2015). The glacially shaped topography is characterized by slopes positioned at a 0 to 70% incline. According to the FAO soil classification system (WRB-IUSS, 2014), the prevailing soil types in the area include Andosols and Histosols (ratio 3:1–4:1), with a dark Ah horizon that originates from volcanic ash and overlies a mineral-rich C horizon (clay dominated). These non-allophanic, humic and acidic soils develop at 0.24 ~ 0.44 m for Andosols and at 0.24 ~ 0.70 m for Histosols. Local Soil Organic Matter (SOM) levels are high, ranging from 0.44 to 0.84 kg kg_{soil}^{-1} (Aucapiña and Marín, 2014); the waterlogging, the formation of organometallic complexes (from Holocene ash deposits), and the low redox potential (a result of the high soil moisture and the wet / cold environment) are responsible for its significant accumulation (Buytaert et al., 2006b). Low bulk density levels, between 0.45 and 0.14 Mg m^{-3}, and a high field capacity of the pore space, between 39 and 90% (mean = 74%), characterize the Andosols and Histosols, respectively (Mosquera et al., 2016a, 2015; Quichimbo et al., 2012). The shallow wetland soils are Histosols and are therefore always saturated.

Our study site is mainly (> 80% coverage) covered by tussock grasses of *Calamagrostis Intermedia* (J. Presl) Steud., which reach heights of between 30 and 80 cm. This native C3 grass is perennial with a ratio of aboveground biomass / necromass ranging from 0.18 to 0.75 (mean = 0.45) and with an estimated sunlit Leaf Area Index (LAI), which ranges between 2.8 and 3.4 $m^2 m^{-2}$ (Hofstede et al., 1995; Nagy et al., 2011). Some areas of the páramo are recurrently affected by grazing, cattle ranching and burning for pasture management (Hofstede et al., 1995; Suarez and Medina, 2001). However, there is no evidence of induced fires or grazing occurring over the past decade in our study area. Local coexistent endemic vegetation includes other grasses, such as *Fetusca* sp. (< 5%), and patches of cushion plants (< 10%) that are sparsely distributed across the wetlands outside of the study fetch (e.g., *Azorella* sp., *Gentiana* sp., *Plantago* sp., *Valeriana* sp., and *Xenophyllum humile* sp.). Finally, remnant patches of small *Polylepis* sp. forests and low shrubs, such as *Weinmannia* sp. and *Buddleia* sp. (< 5%), are also found outside the fetch of the observatory.

The climate of the study area is influenced by the Pacific regime and the predominant continental air masses of the Amazon Basin. Peak values in seasonal rainfall are related to the passage of the Inter Tropical Convergence Zone (ITCZ) through the region. However, as noted by Vuille et al. (2000), sea surface temperature anomalies, such as the El Niño Southern Oscillation (ENSO), do not have a significant influence on the climate at this high elevation. Páramos are also characterized by a lack of thermal seasonality, by steady low temperatures and by prevalent convective and orographic cloud formations (Bendix et al., 2006; Emck, 2007). The average annual temperature is 6.1 °C (max. = 14.2 °C, min. = 0.4 °C), the relative air humidity is 93.6%, and the solar radiation level is 4942 MJ m^{-2} per year (daily average = 13.73 MJ m^{-2} per day), with a noticeable increase in the incoming energy occurring from October to December. Wind speeds follow seasonal patterns and have a monthly mean of 3.21 m s^{-1} from October to March and 4.77 m s^{-1} from June to September. Seasonality is more evident in the levels of precipitation, with the highest levels recorded from January to June (and October) and with an annual mean of 1210 ± 101 mm $year^{-1}$. Thus, bimodal rainfall seasonality is found, similar to other páramo ecosystems (Célleri et al., 2007). Throughout the day, rainfall prevails in the afternoon and almost 30% of all local precipitation is defined as a drizzle, according to Padrón et al. (2015). Hence, our páramo site is characterized by a constant input of water delivered as rain, as is the case for other Neotropical alpine areas (Bendix et al., 2008; Janeau et al., 2015). This climatological information is detailed in Figures S1 and S2 in the supplementary material, showing a monthly climograph (6 years, from Jan. 2012 to Dec. 2017) and annual / monthly wind charts for the same period.

2.2. Experimental setup

To understand the bioclimatic properties of the study site, we used climate data (2012 to 2017) extracted from a conventional automatic weather station (AWS) located 10 m from the EC tower. Measurements taken included the solar radiation, temperature, relative humidity, wind speed and direction, atmospheric pressure and rainfall levels. The quality assessments and controls (QA/QC) of the data were assessed according to Rollenbeck et al. (2016), and data gaps (7% of the total) were filled using an interpolation scheme based on information from a nearby páramo AWS within the same climatic regime (Toreadora site in Cajas National Park, 31 km north and 3995 m a.s.l., data not shown). The AWS data were also used to calculate ETr values (Section 3.6).

Within the 2-year period (March 01, 2016 to February 28, 2018), a 3.6 m EC tower was operational over a site characterized by a gentle slope of 10° and covered by homogeneous and healthy tussock grassland. Atmospheric CO_2 and water vapor (H_2O) fluxes were measured with a LI-7200 enclosed path infrared gas analyzer (IRGA) (LI−COR, Lincoln, NE, USA) running at a constant flow of 15 l min^{-1} delivered through a flow module. Due to the highly humid conditions of the site, an insulated and electrically heated intake tube (LI−COR 7200-050, 71.1 cm in length and 5.33 mm in internal diameter) was installed with the LI-7200. This accessory employed 5 W of power and proved essential for preventing condensation and improving the H_2O frequency response (Metzger et al., 2016). Furthermore, we set this intake tube tilted down at a 5° with a rain cap with a fine screen to prevent water from entering the measurement cell during storm events. In addition, we installed a 2 µm particulate filter into the tube line to prevent insect and dust contamination. We made 3D wind speed / direction and sonic temperature measurements using a GILL-WM Gill New WindMaster 3D Sonic Anemometer (Gill Instruments, Hampshire, UK). The IRGA and sonic anemometer operated at 20 Hz and data were collected from a LI−COR LI-7550 analyzer unit. Complementary micrometeorological sensors were deployed to measure the Net Radiation (Rn), the Photosynthetic Photon Flux Density (PPFD), and the air temperature / relative humidity levels. In addition, the Soil Heat Flux (G) was measured (3 m from the tower) using three heat flux plates while measuring soil moisture / temperature levels with three water content reflectometers (with integrated thermocouples). Detailed characteristics of the aforementioned instrumentation are shown in Table 1. The power supply was provided by two solar panels (250 W each, SolarWorld SW250), which had a MPPT charge controller (SolarEpic Tracer4215BN) and a wind turbine generator (600 W, Windmill DB-600, with an independent MPPT controller, installed at 5 m height, outside of the EC footprint). Both systems were connected in parallel to a battery bank of 550 Ah (5 AGM batteries 12 V & 110 Ah, Power King). The EC tower operation with this hybrid power system proved crucial given the harsh and

Table 1
Instrumentation used in the experiment.

	Variable	Sensors Type and Setup	Unit / Time Step	Accuracy
CO_2 and H_2O Gas Fluxes and Sensible Heat (Fast Sensors) With LI-7550 Analyzer Unit and LI−COR 7200-101 Flow Module	CO_2 and H_2O gas concentration	Enclosed Path IRGA: LI−COR LI-7200 with insulated & heated intake tube at 3.6 m height	ppm and mmol mol^{-1} / 20 Hz	CO_2: Within 1% of reading H_2O: Within 2% of reading
	Wind Speed/Direction/ Sonic temperature	3D Sonic Anemometer: GILL-WM Gill New WindMaster at 3.6 m height	m s^{-1} / 20 Hz	Wind Speed < 1.5%RMS, Direction < 2° (at 12 m s^{-1}) Sonic Temp. < ± 0.5% @ 20 °C
Complementary Micrometeorological sensors (Slow sensors) With Sutron 9210B data logger	Net Radiation	4-Component Net Radiometer: Kipp & Zonen CNR4 at 3.6 m height	W m^{-2} / 1 min	< 1%
	Soil Heat Flux	Three Soil Heat Flux Plates: Hukseflux HFP01 at 5 cm soil depth	W m^{-2} / 1 min	± 0.3%
	Soil Moisture and Temperature	Three Water Content Reflectometers: Stevens Hydra Probe II (each with temperature probes) at 5 cm soil depth	cm^3 cm^{-3} / 1 min °C / 1 min	Stevens Hydra Probe II (Soil moisture ± 2.0%, Soil Temp. ± 0.3 °C)
	Air temperature and relative humidity	Thermometer/Hygrometer: Vaisala HMP155 + Radiation Shield at 3 m height	°C and %RH / 1 min	± 1.7%RH (> 90%RH) / ± 0.226 °C
	PPFD	Quantum Sensor: LI−COR LI190-R at 3.6 m height	µmol s^{-1} m^{-2}	< 1%
Automatic Weather Stations (AWS) (Zhurucay & Toreadora) With Campbell CR1000 data logger	Total Solar Radiation	Pyranometer: Campbell CS300 at 2 m height	W m^{-2} / 5 min	± 5% daily total
	Air temperature and relative humidity	Thermometer/Hygrometer: Campbell CS-215 + Radiation Shield at 2 m height	°C and %RH / 5 min	± 0.3 °C / ± 2% RH
	2D Wind Speed/Direction	Anemometer: Met-One 034BWind Set at 2 m height	m s^{-1} / 5 min	± 0.11 m s^{-1}
	Barometric Pressure	Barometer: Vaisala PTB110 at 1 m height	hPa / 5 min	± 0.3 hPa
	Rainfall	Rain Gage: Texas TE525MM Tipping Bucket with wind shield at 1 m height	mm/ 1 min	± 1%

remote conditions of the study site, where incoming solar energy is often limited due cloudy conditions, but substantial wind power is available most of the time.

2.3. Data preprocessing, QA/QC and instrumental corrections

During the study period, the total loss of flux measurements was 12.7% due to power failures and instrumental errors. Therefore, levels of temporal coverage were superior to the 65% value (annual average) reported by Falge et al. (2001) for other EC sites. Available data on H_2O, CO_2 and energy fluxes from the IRGA and 3D anemometer were binned with an average window of 30 min and were processed using the EddyPro software (version 6.2.0, LI−COR, Lincoln, NE, USA). Here, we applied the following QA/QC: (i) diagnostic flags provided by the instruments, (ii) plausibility limits (sensors and site-related) and (iii) spike removal.

Specific corrections applied included (i) a sectorwise planar fit adjustment for sloped topography and potential canopy inhomogeneities (Wilczak et al., 2001), (ii) cospectra filtering (Mauder and Foken, 2004; Vickers and Mahrt, 1997), (iii) time lag compensations for CO_2 and water vapor (as a function of relative humidity) and (iv) a humidity dependent spectral correction using the method of Fratini et al. (2012). An analysis of the normalized ensemble-averaged hourly cospectra is provided in the Annex S1 of the supplementary materials.

QA/QC values for the half-hourly computed fluxes were determined according to Mauder and Foken (2004) using the 0,1,2 flag system, from which low quality data were removed (flag 2). Table 2 lists the percentages of flagged fluxes.

2.4. Advection-affected fluxes removal, gap filling and uncertainty analysis

Because katabatic flows (generated during calm nights with clear skies) across the slopes of the high Andes (Litt et al., 2015; Trachte et al., 2010), can lead to an underestimation of Reco levels due to the drainage of CO_2 emissions, we performed a flux removal when low turbulence and advection conditions prevailed (i.e., nocturnal katabatic and afternoon anabatic flows) (Aubinet et al., 2012). For this, data with low friction velocity (u*) were filtered by applying the Moving Point Test for threshold detection according to Papale et al. (2006). Then, gaps identified due to data losses resulting from power failures, QA/QC filtering, and low-turbulence filtering were filled via Marginal Distribution Sampling (MDS) using the REddyProc R-package (Reichstein et al., 2017, 2005).

We estimated the uncertainty error induced by gap filling using a bootstrapping technique (resampling with replacement) and by creating a dataset of pseudoreplicates. The differences between the high and low threshold estimates (95% and 5% quantiles of the bootstrapped uncertainty distribution) corresponded to the uncertainty level (introduced by the uncertain estimate of the u* threshold). We also calculated the random error of the original CO_2 fluxes according to Finkelstein and Sims' (2001) method.

To provide insights about the occurrence of nocturnal advection in our site, we included an analysis of the nocturnal turbulence (u*) and its relationship to nocturnal C fluxes (Annex S3). Finally, we tested the sensitivity of the NEE balance to the u* threshold-based filtering and gap filling processes.

Table 2
Flux quality flags. Flag 2 data were discarded for analysis purposes.

Quality Flags	Sensible Heat	Latent Heat	CO_2 flux	H_2O flux
Percentage Flag 0 (High Quality)	12.7%	9.9%	13.6%	9.9%
Percentage Flag 1 (Intermediate Quality)	68.7%	65.5%	72.1%	65.5%
Percentage Flag 2 (Poor Quality)	18.6%	24.6%	14.2%	24.6%

2.5. Energy balance and footprint analyses

The suitability of the flux results is also based on the Energy Balance Closure (EBC) level and our footprint analysis of the source of fluxes. EBC was conducted from Rn, G, Latent Heat (LE) and Sensible Heat (H) values and gap-filled data were excluded to avoid bias. Hence, turbulent fluxes (H + LE) should be approximately equal to the amount of available energy (Rn – G) (linear regression). For this computation, Rn was corrected by slope and aspect conditions (slope = 10° and aspect = 145° southeast) to force the surface-normal energy incoming into the system following the methodology developed by Olmo et al. (1999) and detailed in Leuning et al. (2012) and Serrano-Ortiz et al. (2016). We applied this correction under relatively sunny conditions using a sky clearness index (Kt) of greater than 0.7 to avoid making unnecessary corrections when diffuse-irradiance sky conditions due cloudy conditions that characterize the páramo were present. Kt values were calculated to be the ratio between the incoming shortwave radiation (Rs) (pyranometer measurements) and the modeled Extra-terrestrial Radiation (Ra), following Duffie and Beckman (2013); the resulting Kt values were found to account for 9.4% of the Rn observations. Final G fluxes accounted for the direct measurements with the plates (Gs), plus the heat storage estimation (G_{ST}) of Mayocchi and Bristow (1995). Energy flux densities for relatively sunny days were analyzed as well.

A Flux Footprint Prediction (FFP) based on the method of Kljun et al. (2015) was conducted to estimate the spatial origins of the flux and to exclude potential flux sources of nontussock grass vegetation. The FFP demonstrated the existence of unidirectional fluxes (northeast) with minor contributions from the southwest. Here, 80% of the footprint was found within 100 ~ 130 m of the tower, covering a homogeneous grassland area of approximately 1.6 ha (97.5% of grassland cover, 0.4 ~ 0.8 m canopy height), which had a low level of topographical variability. Thus, less than 2.5% of the data were excluded after the FFP assessment. The analysis is described in detail in Annex S2 of the supplementary material.

2.6. Flux calculations and CO_2 light / temperature–response parameterization

The NEE is a crucial indicator for understanding the páramo's role as a C source / sink by aggregation over time (i.e., daily, seasonally and yearly). For a long-term analysis, the calculation of the NEE, is only achievable through continuous flux detection (the EC technique). Consequently, the NEE was divided into its main components of GPP and Reco (where: NEE = GPP – Reco). For this purpose, we used a regression of nighttime NEE and soil temperature (Lloyd and Taylor, 1994), in which the latter was taken as a proxy for the daily rates of Reco. Then, GPP was estimated to be the difference between NEE and Reco. Finally, negative nighttime GPP values were set to zero. Flux partitioning was conducted using the R REddyProc package (Reichstein et al., 2017), and NEE, GPP and Reco were aggregated in daily, monthly and annual sums to explore the C budgets over different time periods.

Furthermore, we parameterized specific equations from half-hourly datasets to represent the CO_2 response to light and soil temperature, a process that is applicable to non-EC monitored sites that have only conventional meteorological measurements available. For these sites, NEE was fitted to a Mitscherlich equation form (Falge et al., 2001) in which GPP_{max} is the diurnal maximum productivity level (or max. C uptake when compared with PPFD). The model was adjusted, with days showing a minimum midday uptake of –2 μmol m^{-2} s^{-1}. The Mitscherlich formulae were used instead of the traditional Michaelis and Menten (rectangular hyperbola) models to prevent an overestimation of NEE (at light saturation) (Stoy et al., 2014). Based on the full half-hourly dataset, GPP was linearly correlated with NEE and Reco was represented by a polynomial correlation with soil temperature (T_{soil}).

By convention, the positive Net Exchange (+NEE) represents the negative Net Ecosystem Production (–NEP) according to Chapin et al. (2006). Therefore, we used NEP instead of NEE to compare the positive C assimilation in the ecosystem (sink), the GPP and the Reco against control variables such as PPFD, soil temperature and soil moisture. For this purpose, we calculated Spearman's correlations (with a *t*-test for each case) for the full period and for days with positive NEP (> +0.10) and negative NEP (< –0.10) values. Correlations with p-values > 0.05 were considered to be insignificant.

2.7. The study period in context of longer-term observations

To bring our shorter-term measurements in line with the longer-term climate conditions in the páramo, a 48-year climate dataset (monthly temperature and precipitation for 1964–2011) from the nearby páramo AWS El Labrado (40 km north-east and 3335 m a.s.l., data provided by the National Institute of Meteorology and Hydrology of Ecuador INAMHI) was compared with the available measurements from Zhurucay (6-year) and, in particular, with the 2-year flux monitoring data. Using this dataset, the integrated anomalies in precipitation and temperature were determined for the complete period (54 years) using the well-known Standardized Precipitation Evapotranspiration Index (SPEI) (Beguería et al., 2014; Vicente-Serrano et al., 2010). The SPEI is advantageous for describing the meteorological dryness / wetness because it combines multiscalar characteristics with a sensitivity to temperature fluctuations. A 1-month-based SPEI scale served to classify the historical drought or excess water conditions of our study period. Prior to the establishment of this scale an adjustment for the páramo's specific altitudinal temperature lapse rate (according to Córdova et al. (2016)), was adopted to fit the El Labrado dataset to the elevation of Zhurucay.

Furthermore, we obtained a 19-year dataset of satellite GPP observations from the MODIS product MOD17A2H (MODIS/TERRA Gross Primary Productivity, version 6, 500 m of resolution, 8-day composite for 2000–2018, available from the Land Processes Distributed Active Archive Center (LP DAAC)) for the correspondent pixel of our EC footprint. Cloud-contaminated images (low QA/QC of the product) were excluded from the analysis prior to obtaining daily averages for each month to compare the results to our GPP estimations.

2.8. Evapotranspiration and Kc

The EC method produced measurements of ETa, which were derived from the air density (ρ), vertical wind speed (*w*) and water vapor mixing ratio (water vapor mass divided by dry air mass = *q*) values, according to Eq. (1):

$$ET_a = \bar{\rho} * \overline{w' * q'} \quad (1)$$

This flux consists of transpiration, the evaporation of intercepted rain / fog and the evaporation from soil surfaces, and it is extremely useful for understanding water availability and carbon / water coupling in natural and disturbed biomes. As was done for NEE fluxes, diurnal half-hourly ETa observations affected by power failures, QA/QC filtering and low turbulence were identified and discarded (30.7% of data), following Papale et al. (2006). Then, the gaps were filled via the MDS technique and the corresponding uncertainty was retrieved. ETa observations were aggregated at daily, monthly and annual time steps and were compared with ETr values calculated from standard (and frequently used) methods of FAO56 PM Penman-Monteith reference evapotranspiration (grass-based) (Allen et al., 1998) and ASCE-ERWI standardized reference evapotranspiration (alfalfa-based) calculation (ASCE-ERWI, 2001). Finally, the Kc values for the páramo tussock grasses were obtained from the ETa / ETr ratio for both ETr methods (considering the less humid and wet periods of the site) and were then contrasted with other Kc values reported in the literature.

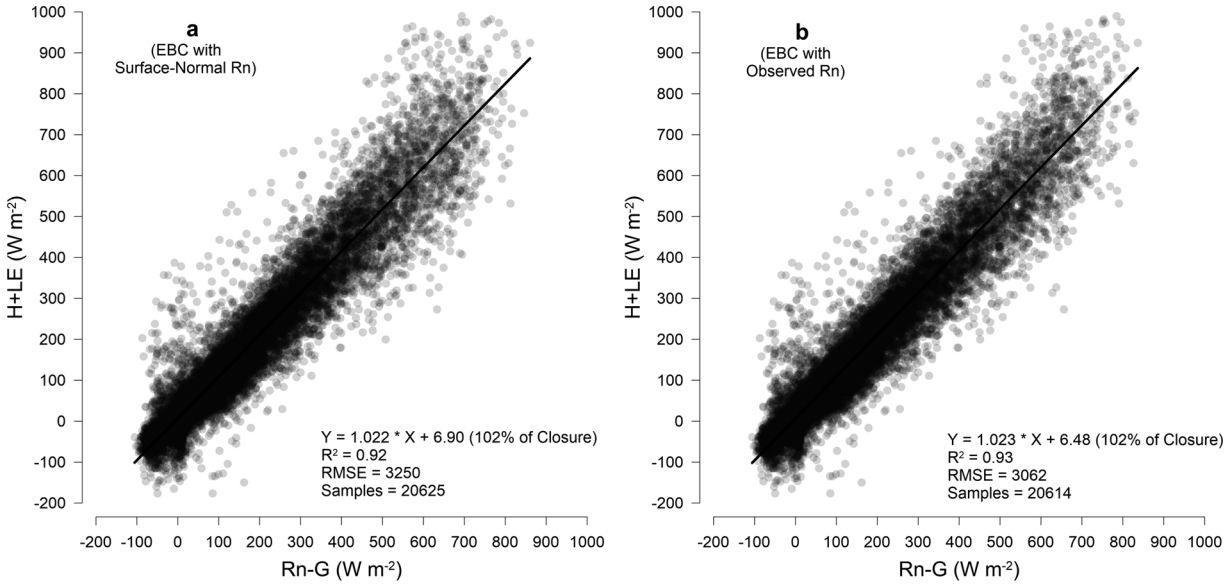

Fig. 2. EBC for the study site: (2a) EBC with an Rn Surface-Normal correction (2b) EBC with uncorrected Rn (direct observation). No gap-filled data were used.

3. Results and discussion

3.1. EBC and energy flux densities

Fig. 2 shows two EBC scenarios: (2a) EBC with an Rn Surface-normal correction and (2b) EBC with direct Rn observations (i.e., without correction). For both cases, we obtained a regression slope of 1.02, which represents an outstanding closure comparable to other tropical sites with moist environments (Cabral et al., 2015, 2010). We also observed a linear intercept of 6.5 ~ 6.9 W m^{-2}, a high correlation R^2 value of 0.92 ~ 0.93, and analogous values of RMSE.

While some studies encourage the geometrically-based adjustment of Rn for EC experiments of steep terrain (Hammerle et al., 2007; Olmo et al., 1999; Wohlfahrt et al., 2016), our findings demonstrate that for our location (which has a high diffuse radiation dominance), a surface-normal correction does not significantly improve the EBC.

Fig. 3 shows the energy flux densities for the relatively cloud-free days (average of 9 days) during a less humid / high radiation period (August 2016) and during a wet / low radiation period (January 2017). The Rn Surface-Normal corrected and Rn observed curves are shown, as are the LE, H, G and residuals of the corrected or uncorrected Rn scenarios (Res_{RnSN} and Res_{Rn}). Standard deviation bars are also shown in the figure.

During the less humid month (3a), the sensible heat doubled the latent heat density (H_{mean} = 127.6 W m^{-2} versus LE_{mean} = 64.0 W m^{-2}). However, differences between H and LE during the wet month (3b) were less significant (H_{mean} = 89.6 W m^{-2} versus LE_{mean} = 93.0 W m^{-2}). This can be attributed to an increase in the humidity of the environment and the soil due to higher levels of precipitation. Finally, differences in the available energy (Rn_{SN} – G), the turbulent flux (H + LE), and the residuals (Res_{RnSN}) were measured to be 10.5%, 4.7% and 30.1% higher, respectively, in the less humid period than in the wet period. Additionally, the deviations of all of the density curves (SD) were found to be notably higher for the wet period.

The 2-year of energy fluxes analysis shows daily averages of Rn_{SN} = 102.2 ± 40.4 W m^{-2}, H = 64.4 ± 39.2 W m^{-2}, LE = 57.7 ± 27.3 W m^{-2}, and G = 0.5 ± 5.4 W m^{-2} with residuals of (Res_{RnSN}) = –15.0 ± 36.1 W m^{-2}. However, the diurnal partitioning of the net available energy (07:00 – 18:00) into H and LE was measured to be 55.0% and 43.5%, respectively. Therefore, a significant

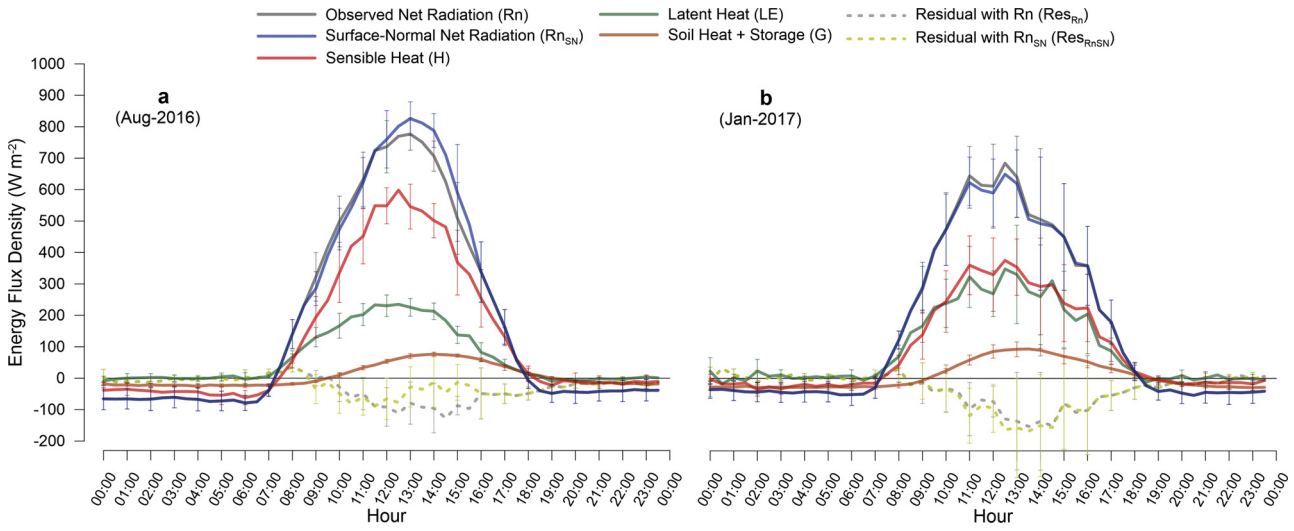

Fig. 3. Hourly energy flux densities on cloud-free days for (3a) a less humid / high radiation month (August 2016) and (3b) a wet / low radiation month (January 2017), with error bars.

amount of the available energy is used for atmospheric heating.

3.2. NEE measurements and partition-derived carbon fluxes (GPP, Reco)

NEE (μmol m^{-2} s^{-1}) half-hourly fluxes were obtained from the available CO_2 flux measurements (after the QA/QC process). Data affected by low turbulence and advective conditions were filtered (25.5% of NEE) (via u* threshold-detection) and friction velocity thresholds of u* = 0.344 and u* = 0.321 were applied, for the first and second year, respectively. The NEE half-hourly means for the first and second year were 0.33 ± 3.86 and 0.19 ± 3.77 μmol m^{-2} s^{-1}, respectively. The correspondent uncertainty averages were 0.02 ± 0.68 and 0.02 ± 0.56 μmol m^{-2} s^{-1} (6.9% and 12.6% of the induced error to the gap-filled data, respectively). Following the method of Finkelstein and Sims' (2001), original CO_2 half-hourly fluxes had a mean of 0.07 ± 3.97 μmol m^{-2} s^{-1}, with an average random error of 0.02 ± 0.49 μmol m^{-2} s^{-1} (28% of the error). These uncertainties are lower than those reported by Baldocchi et al. (2001) for other FLUXNET sites (0.4 μmol m^{-2} s^{-1}). The analysis of the nighttime turbulence (u*) and its relationship with nighttime C fluxes, presented in the Annex S3 of the supplementary materials, demonstrates that the selected u* thresholds used in the data filtering can reduce the possibility of an underestimation of nighttime Reco.

The GPP and Reco modeled by the partitioning process developed by Reichstein et al. (2005) are shown in Fig. 4. The half-hourly NEE fingerprint is shown in Fig. 4a and the daily aggregated NEE, GPP and Reco fluxes are shown in Fig. 4b.

In this figure, the NEE fingerprint (Fig. 4a) shows consistent levels of diurnal-nocturnal fluctuation from sunrise (approx. 07:10) to sunset (approx. 18:05) without intra-annual seasonality or a noticeable degree of C uptake (by the ecosystem) from 09:00 to 15:00. The C fixation process tended to decline in the late afternoon hours as was expected due to the frequent afternoon-cloudiness of the páramo, which limits photosynthesis earlier in the day than is the case under cloud-free conditions. The hourly daytime NEE mean was –2.97 ± 3.01 μmol m^{-2} s^{-1} (max. = –13.55 μmol m^{-2} s^{-1}) and the nighttime NEE mean was measured to be +3.23 ± 1.04 μmol m^{-2} s^{-1} (max. = +19.56 μmol m^{-2} s^{-1}). During a few days in June, October, November and December 2016-17, we observed higher values of C release at night, likely because these days preceded less humid periods and were followed by rain events, conditions that can promote respiration.

Daily aggregations of fluxes (Fig. 4b) show predominantly positive NEE values with a daily mean of +0.27 ± 0.58 gC m^{-2} day^{-1}, a maximum of +2.50 and a minimum of –1.36 gC m^{-2} day^{-1}. In total, 484 days registered positive values and 246 days registered negative NEE values, meaning that for only 34% of the time, the páramo acted as a weak C sink. On the other hand, partition-retrieved GPP values reached a mean of 3.21 ± 0.86 gC m^{-2} day^{-1}, (max. = 7.98, min. = 0.45) and the Reco mean reached 3.48 ± 0.76 gC m^{-2} day^{-1}, (max. = 7.47, min. = 0.69). Very few studies have evaluated observations (or validated model estimations) of atmospheric C flux in the páramo. For instance, McKnight et al. (2017) obtained a Reco flux average of 4.58 ± 0.22 μmol m^{-2} s^{-1} from midday measurements (between 10:00 and 14:00) by applying the soil CO_2 flux chamber technique to a similar biome (Mazar Wildlife Reserve: 3450 m a.s.l. 91 km east of Zhurucay). This Reco value is 39% higher than our observations (3.30 ± 0.81 μmol m^{-2} s^{-1}). Sánchez et al. (2017) used diurnal NEE measurements, combined with simulated nocturnal Reco and inferred GPP values, derived from a CO_2 IRGA with a custom-made transparent chamber for NEE and a sunlight block fixture to simulate

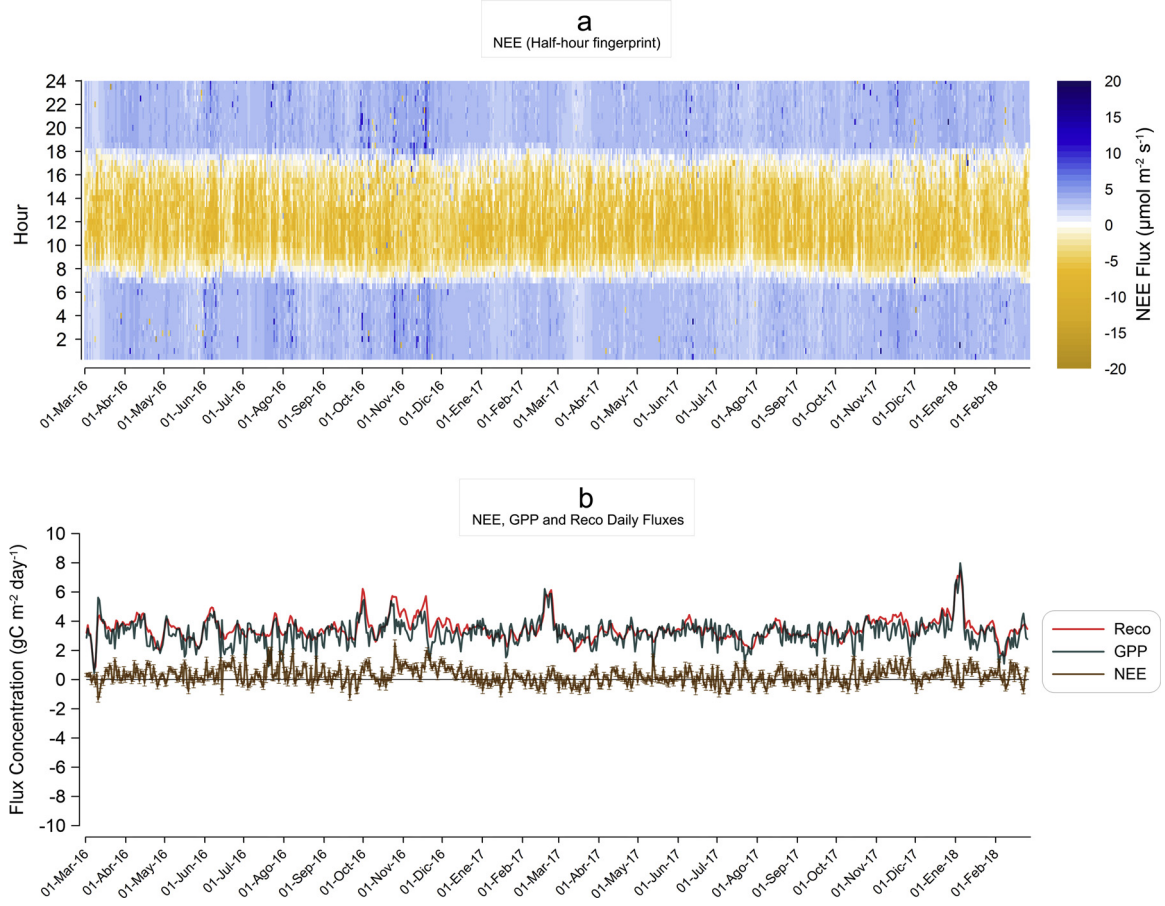

Fig. 4. Half-hourly NEE fingerprint (4a) and daily aggregated NEE, GPP and Reco fluxes (4b) for the study period. The hourly standard deviation of NEE is shown as bars.

Table 3
Monthly and annual NEE, GPP and Reco fluxes.

	NEE	GPP	Reco
Monthly Average with SD* ($gC\ m^{-2}\ month^{-1}$)	8.2 ± 7.7	97.6 ± 10.7	105.8 ± 13.9
Wet Period Average **	6.2 ± 6.2	98.9 ± 12.5	105.1 ± 14.9
Less humid Period Average ***	11.1 ± 9.0	95.7 ± 7.9	106.8 ± 13.2
Difference Wet vs. Less humid (%)	80.8%	–3.3%	1.7%
First year Sum ($gC\ m^{-2} year^{-1}$)	128.8	1175.1	1303.7
Second year Sum ($gC\ m^{-2} year^{-1}$)	68.7	1166.4	1235.2

* SD Standard deviation.
** Wet period contemplated: January, February, March, April, May, June and October.
*** Less humid period contemplated: July, August, September, November and December.

dark respiration for an undisturbed peatland site (cushions and lawns over histosols) in the Cayambe-Coca National Park (4260 m a.s.l., near the active volcanic highlands of northern Ecuador). Values reported from this survey (09:00 – 16:00 during dry-days) are as follows: NEE = –0.69 ± 0.08 gC $m^{-2} hour^{-1}$, Reco = 0.66 ± 0.06 gC $m^{-2} hour^{-1}$ and GPP = 1.35 ± 0.12 gC $m^{-2} hour^{-1}$. In this study, the authors noted that CO_2 losses might be higher if nighttime respiration were measured. Our corresponding daytime NEE reached –0.18 ± 0.09 gC $m^{-2} hour^{-1}$, the nighttime Reco reached 0.14 ± 0.03 gC $m^{-2} hour^{-1}$, and the GPP (full dataset) reached 0.33 ± 0.10 gC $m^{-2} hour^{-1}$. Our values are clearly lower than those for the Cayambe-Coca site. It should be stressed that these studies only used daytime sampling methods in a short-term monitoring period, rather than the EC technique, which performs a continuous (diurnal / nocturnal) monitoring of fluxes, surveying the whole ecosystem (Baldocchi, 2003).

Monthly and annual aggregations of C fluxes are shown in Table 3. We found that NEE, GPP and Reco monthly averages for the less humid period were higher than those for the wet period, especially for NEE.

In investigating analogous carbon-exchange studies of the Ecuadorian páramos, Minaya et al. (2016) retrieved monthly GPP estimations by applying the Biome-BGC model and validated the model with ground-based GPP values (derived from aboveground biomass and C stock ratios) for the Antisana Ecological Reserve (near to Cayambe-Coca). In their study, low elevation sampling areas (4000–4200 m a.s.l.) showed a modeled GPP of between 80 and 120 gC $m^{-2}\ month^{-1}$ and ground-based GPP values of approximately 95 to 100 gC $m^{-2}\ month^{-1}$. The latter results are similar to our estimates.

We found that our site is a source of carbon, with annual NEE budgets of +128.8 gC $m^{-2} year^{-1}$ for the first year, +68.7 gC $m^{-2} year^{-1}$ for the second year, and annual uncertainties (attributed to u* threshold removal and gap filling) of 4.33 gC $m^{-2} year^{-1}$ and 3.41 gC $m^{-2} year^{-1}$, respectively. The C balance shown in Table 3 is sensitive to the u* threshold-based filtering and gap filling. To quantify this sensitivity we increased the u* threshold by 20% (i.e., from 0.344 to 0.413 m s^{-1} for the first year and from 0.321 to 0.385 m s^{-1} for the second year) and then recalculated the annual budgets of NEE. This modification increased the NEE balance by 2.64 gC $m^{-2} year^{-1}$ and 1.92 gC $m^{-2} year^{-1}$, respectively (which represents 61% and 56% of the annual aforementioned uncertainty). Therefore, it is unlikely that higher u* threshold values can affect the NEE budget beyond the uncertainty level.

Respiration clearly exceeded gross primary productivity (11% and 6%, first and second year, respectively). Consequently, the páramo behaved as a CO_2 source for this particular period. This finding can be explained by several key ecosystem characteristics: (i) páramo soils release CO_2 depending on the stability of SOM to decomposition (Tonneijck et al., 2010), but this is strongly dependent on local alpine inhibition factors (i.e., limited radiation, low temperatures, high humidity levels and mineral inputs) that not yet fully understood (Hribljan et al., 2016); (ii) heterotrophic ($Reco_H$) and autotrophic ($Reco_A$) respiration mechanisms have been rarely investigated for this harsh ecosystem; however, a study of the $Reco_H$ of páramo soils in Colombia (Curiel Yuste et al., 2017) reported a high sensitivity of CO_2 emissions to changes in soil temperature (unaffected by soil water saturation). Thus, given persistent diurnal-nocturnal variations in soil temperature found at our site (max. = 20.3 °C, and min. = 4.8 °C), the daytime $Reco_H$ rates may potentially overcome the CO_2 sequestration rates; and (iii) the photosynthesis of tussock grasses (the dominant species, which possesses a low biomass / necromass ratio) is strongly affected by the limitations of sunlight in the cloudy páramo. The phenology and water use efficiency of this plant species are still unexplored.

Table 4 compares the annual C budgets (EC technique-based) of globally distributed tropical, mid-high elevation, and high-latitude (tundra) grasslands (with similar characteristics as the system studied here) to values obtained in this study.

Certainly, most undisturbed prealpine and alpine grasslands (e.g., Niwot Ridge, Qinghai-Tibetan Plateau and Monte Bondone) and to a lesser degree the Australian subalpine grasslands (Dargo) act as strong C sources. These ecosystems are, however, subject to seasonality and their water supplies are dependent on snowmelt during the winter (rainfall is also scarce). Additionally, some of these biomes share related species of mid-tall grasses (*Carex*, *Poacea* and *Eriophorum* sp.). On the other hand, arctic tundra sites (e.g., Imnavait Creek and Atqasuk) mostly act as weak C sources. Despite having a significant water surplus, these biomes have a considerable deficit of incoming solar radiation, which limits C fixation during a significant period of the year. Regardless of the mid-elevation location of the Cerrado grassland in Brazil (which has a large water supply and is closer in latitude to our site), this biome acts as a C sink, unlike the Panama pasture (Sardinilla), which serves as a strong source of CO_2. Finally, our site shows annual GPP levels as high as those of other source-type ecosystems (Monte Bondone and Sardinilla) and nearly as high as those of the Qinghai-Tibetan Plateau.

Similarly, páramo soil and vegetation can release significant CO_2 relative to other low-elevation tropical ecosystems, as is the case for boreal and arctic tundra biomes where NEP decrements are greater than GPP decrements according to latitude (releasing larger emissions relative to respiration). This behavior can remain constant over time (possibly interannually), as the seasonal variability in GPP and Reco levels for the tropics is lower than that of other biomes, as noted by Falge et al. (2002), given the dominant role of cloudiness in photosynthesis modulation for tropical regions as stated by Baldocchi et al. (2018) in a review of numerous FLUXNET sites.

Estimates of páramo soil age ranging from 6675 to 8270 years before present (B.P.) were reported by Hribljan et al. (2016) for grasslands of the Cayambe-Coca National Park, with historical C accumulation rates of up to 23 gC $m^{-2} year^{-1}$ and a soil C storage of 183 kgC m^{-2}. Jantz and Behling (2012) reported an estimate of soil age of 8428 ± 41 years B.P. for the Quimsacocha Tres-Lagunas site (2 km north of our site, with the estimate based on pollen and charcoal records). Their results indicate that cooler and humid conditions (late-Holocene 2200 years B.P.) were optimal for the soil C accumulation. However, a stronger human influence is also detected during the last 200 years B.P. In spite of the alterations in C-dynamics due to natural processes, such as volcanic activity or preindustrial-era climatic shifts, whether some páramo locations (such as our site) are experiencing recent C stock depletion (in contrast to its longer-term accumulation capacity) remains unclear. To understand these processes, a longer-term observational period of EC exchange measurements combined with of the study of soil and vegetation-level C stocks and diurnal / nocturnal fluxes is urgently needed.

Table 4
Comparison of Zhurucay annual C budgets (average) to other tropical, mid-high elevation, and high-latitude (tundra) grasslands around the globe (EC experiments only).

	Location (Country)	World Ecoregion*	Elev. (m a.s.l.)	Lat. / Long.	Biome / Dominant species	Seasonality	SWC (%) or Water Table (cm)	Period	NEE ($gC\ m^{-2}\ year^{-1}$)	GPP ($gC\ m^{-2}\ year^{-1}$)	Reco ($gC\ m^{-2}\ year^{-1}$)	Reference
Tropical	**Zhurucay Páramo** (Ecuador)	Northern Andean páramo	3765	3.06 S / 79.24 W	Alpine Tundra / *Calamagrostis I.* sp., *Fetusca* sp.	No	74%	2016-2018	+98.8	1170.8	1269.5	(Present study)
	Brazilian Cerrado (Brazil)	Cerrado	1060	15.55 S / 47.54 W	Wet Grassland / *Axonopus C.* sp.	No	> 80%	2005-2006	–83.9	1459.3	1375.4	(Meirelles et al., 2015)
	Sardinilla ** (Panama)	Isthmian-Atlantic moist forests	70	9.32 N / 79.63 W	Pasture / *Paspalum D.* sp., *Rhynchospora N.* sp.	No	~39%	2007-2009	+261.0	2345.0	2606.0	(Wolf et al., 2011)
Mid-High Elevation	**Niwot Ridge** (USA)	Colorado Rockies forests	3500	40.05 N / 105.58 W	Alpine Tundra / *Carex R.* sp., *Paronychia P.* sp.	Yes	–	2008-2012	+175.0	124.0	329.0	(Knowles et al., 2015a)
	Qinghai-Tibetan Plateau (China)	Southeast Tibet shrublands and meadows	3250	37.58 N / 101.33 E	Alpine Meadow / *Kobresia. T.* sp., *Carex P.*sp.	Yes	30 cm	2004-2006	+106.1	629.9	737.3	(Zhao et al., 2009)
	Dargo (Australia)	Australian Alps montane grasslands	1648	37.13 S / 147.17 E	Subalpine Grassland / *Poa Hiemata* sp.	Yes	–	2007-2014	+18.0	95.0	78.0	(Beringer et al., 2016)
	Monte Bondone (Italy)	Alps conifer and mixed forests	1563	46.02 N / 11.03 E	Subalpine Grassland / *Molinia C.* sp., *Carex R. and N.* sp., *Eriophorum V.* sp.	Yes	74%	2012-2014	+180.7	1191.0	1307.7	(Pullens et al., 2016)
	Graswang (Germany)	Western European broadleaf forests	864	47.57 N / 11.03 E	Subalpine Grassland / *Plantago L.* sp., *Trifolium R.* sp.	Yes	~50%	2011-2014	–226.0	1518.0	1293.0	(Zeeman et al., 2017)
Tundra	**Imnavait Creek** (Alaska, USA)	Artic tussock tundra	930	68.61 N / 149.30 W	Arctic Tussock Tundra / *Eriophorum V.* sp., *Sphagnum* sp.	Yes	–	2013-2014	+30	–	–	(Euskirchen et al., 2017)
	Atqasuk (Alaska, USA)	Artic coastal tundra	24	70.46 N / 157.40 W	Arctic Tundra / *Eriophorum V.* sp., *Carex B.* sp., *Vaccinium V.* sp.	Yes	–	2006	+13.6	–	–	(Oechel et al., 2014)
Other	**Auchencorth Moss** (Scotland)	Celtic broadleaf forests	267	55.79 N / 3.24 W	Peatland / *Deschampsia F.* sp., *Eriophorum V.* sp.	Yes	4 cm	2002-2013	–64.1	–	–	(Helfter et al., 2015)

NEE, GPP and Reco are reported as annual averages. Negative NEE indicates a C sink ecosystem, Positive NEE a C source ecosystem.
SWC = Soil Water Content.
* Retrieved from the Terrestrial Ecoregions of the World (TEOW) map (Olson et al., 2001).
** Values of Sardinilla are reported for 2008.

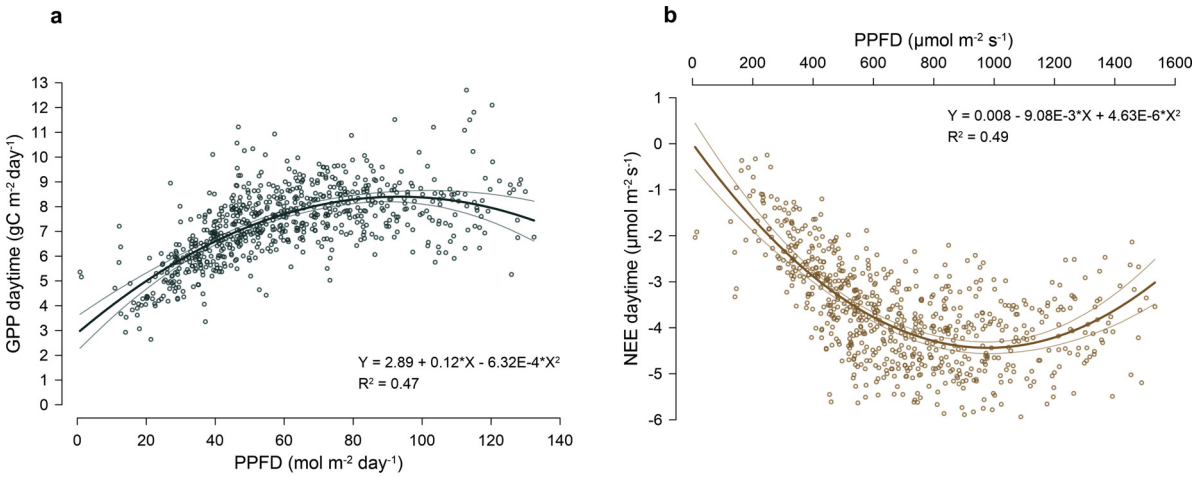

Fig. 5. Nonlinear fit of diurnal GPP versus PPFD (5a) and average diurnal NEE versus PPFD (5b) with 95% confidence bands (thin lines).

3.3. NEE / GPP light–response and carbon exchange models

As photosynthesis and C fixation are limited by photon availability, the productivity of the páramo must be related to sunlight levels (see Fig. 5). Hence, in Fig. 5a, the total diurnal GPP is correlated with total daily PPFD, and shows a positive correlation with $R^2 = 0.47$ (nonlinear model with 95% confidence band), which demonstrates that GPP proportionally increased as PPFD increased until the GPP reached saturation (8.5 gC m^{-2} day^{-1}, at 96.0 mol m^{-2} day^{-1}).

Furthermore, Fig. 5b shows the relationship between the average diurnal NEE and the average PPFD (in µmol m^{-2} s^{-1}, at the 95% confidence level), and depicts a positive correlation ($R^2 = 0.49$) between the C uptake (negative NEE) and the photon flux. NEE was saturated at an emission level of –4.5 µmol m^{-2} s^{-1} and at 990 µmol m^{-2} s^{-1} of PPFD.

Our parameterization of C fluxes to light and soil temperature responses for this ecosystem is presented in Eqs. (2)–(4) as follows:

$$NEE = GPP_{max} * (1 - e^{(\frac{0.035 * PPFD}{GPP_{max}})}) + 3.192\,;\ (R^2 = 0.95,\ p < 0.05) \quad (2)$$

$$GPP = -0.992 * NEE + 3.350\,;\ (R^2 = 0.95,\ p < 0.05) \quad (3)$$

$$Reco = 3.207 - 0.209 * T_{soil} + 0.019 * {T_{soil}}^2\,;\ (R^2 = 0.40,\ p < 0.05) \quad (4)$$

In Eq. (2), the apparent quantum yield coefficient (0.035) and the dark respiration coefficient (3.192) are similar to those reported by Ruimy et al. (1995) for grasslands. These equations are suitable for the empirical estimation of C fluxes in similar páramo locations, where, for instance, PPFD can be inferred from the Rs of conventional AWSs. However, the development of site-specific equations is recommended for more heterogeneous locations.

3.4. CO_2 fluxes versus climatic / biophysical controls

Fig. 6 shows the analyses of the correlations between CO_2 assimilation in the ecosystem (NEP, explained in Section 2.6), GPP and Reco fluxes and specific climatic / biophysical controls: daily PPFD, soil water content and soil temperature.

For the full period, NEP showed a moderate correlation with GPP and PPFD, a weak or no relationship with soil moisture and soil temperature, and an inverse relationship with Reco. This behavior was undetermined for correlations with $p < 0.05$. On the other hand, GPP cannot be correlated with Reco, given that one is derived from the other (Vickers et al., 2009). Full period GPP was strongly related to PPFD and soil temperature. An inverse correlation between full period GPP and soil water content was found for the three datasets. These findings suggest that limited CO_2 sequestration periods in the páramo (+NEP and GPP) can be promoted by increases in PPFD but are inhibited by increases in soil moisture. Reco also showed a positive correlation with PPFD and soil temperature for the whole period and an especially strong correlation for negative NEP days, as well as an inverse relationship with soil water content. Like those for NEP and GPP, these findings also suggest that C emissions can be promoted through increases in light and soil temperature and through strong reductions in soil water content (a rare occurrence in the páramo). Finally, the relationship between PPFD and the soil water content was inverse and proportional to the soil temperature, and the soil water content was inversely proportional to the soil temperature. Figure S6 in the supplementary material illustrates a daily time series for NEP, GPP and Reco versus soil temperature, water content and rain depth for the study period.

3.5. The study period in comparison to longer-term environmental observations

Fig. 7a depicts (i) the long-term temperature and precipitation series for the El Labrado climate station (INAMHI) as monthly averages with standard deviation, (ii) the 6-year monthly climate data from Zhurucay highlighting the flux measurement periods, and (iii) the NEE, GPP and Reco monthly sums. The overall variability in the long-term temperature and rainfall is consistent with that of the Zhurucay climate series, in spite of the difference in altitudinal temperature at El Labrado. Monthly scale fluxes have an unclear relationship with climatic variables. However, for January and February 2016 and March 2017 the ecosystem exhibits a weak uptake of CO_2 (–0.4, –0.6 and –4.7 gC m^{-2} $month^{-1}$, respectively), which is probably associated with the precedent decline in rainfall and the subsequent radiation increase in the system.

In Fig. 7b, the 1-month-based SPEI interestingly shows that the period of EC monitoring can be classified as moderate wet (the beginning of each year) to moderate dry (the 5 intermediate months of each year), according to the categorization of McKee et al. (1993) and the World Meteorological Organization (2012) for meteorological dryness / wetness. Finally, Fig. 7c reveals a relative consistency and similar magnitude of the MODIS GPP long-term observations (the daily mean of which is 3.33 ± 0.14 gC m^{-2} day^{-1}), when compared to our EC-based GPP estimations (the daily mean of which is 3.21 ± 0.21 gC m^{-2} day^{-1}), in spite of the low regression coefficient found.

These results provide an insight to how representative our study period is of the longer-term dynamics of the páramo's climate conditions for the last 54 years and confirm that our flux measurements were acquired in the absence of drought or excess water anomalies.

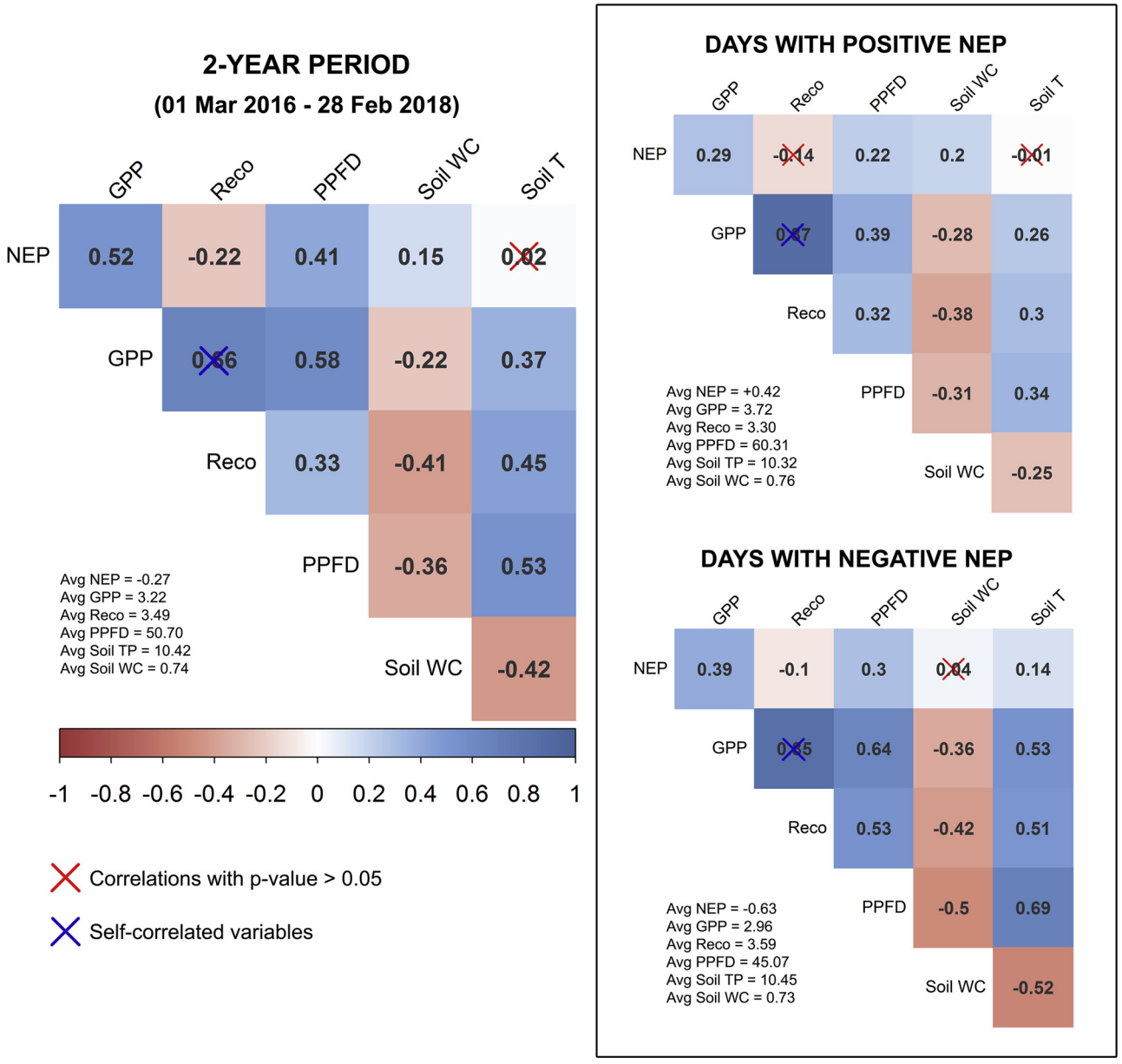

Fig. 6. Spearman's correlograms for NEP, GPP, Reco, PPFD, soil water content and soil temperature. Days with positive and negative NEP are analyzed independently. Correlations with p-value > 0.05 are cross-marked.

3.6. Evapotranspiration

During the study period, the mean-hourly ET reached 0.13 ± 0.12 mm hour^{-1} with a mean uncertainty of 0.001 ± 0.004 mm hour^{-1} for the gap-filled values. Therefore, only 0.9% of the error was introduced to these data as a result of the gap filling process. Additionally, the random error for the water fluxes calculated following the Finkelstein and Sims' (2001) method was of 0.13 ± 0.21 µmol m^{-2} s^{-1}, which is equivalent to 9.8% of the H_2O half-hourly mean (1.31 ± 1.92 µmol m^{-2} s^{-1}). Thus, these biases hardly affected the monthly and annual ET aggregations (as shown in Section 3.2 for NEE).

Fig. 8a depicts the hourly dispersion between ETa and the modeled ETr from FAO56 (Allen et al., 1998) and ASCE (ASCE-ERWI, 2001) methods, and Fig. 8b shows the daily ET values by notched boxplots (95% confidence interval). In Fig. 8a, we illustrate the daytime course of ET during four days in August 2016 (clear and cloudy conditions). The modeled ETr tended to overestimate the ETa fluctuations, especially for ETr (ASCE). The ETa flux lags during sunshine hours and is suppressed prior to sunset, particularly on sunny days. It is important to note that the general ETr models of FAO56 and ASCE do not account for a surface-normal correction of solar radiation by default.

The linear fitting of the available half-hourly data exhibits good closure (slope) between ETa and ETr (FAO56) but confirms that ETr (ASCE) is overestimated; however, both show similar regression coefficients.

Daily means of ET for the 2-year period were measured to be: ETa = 1.74 ± 0.28 mm day^{-1} (max. = 5.1, min. = 0.3), ETr (FAO56) = 1.93 ± 0.42 mm day^{-1} (max. = 5.4, min. = 0.0), and ETr (ASCE) = 2.23 ± 0.49 mm day^{-1} (max. = 7.6, min. = 0.3). Therefore, the values were overestimated by 10.6% and 27.9% for the FAO56 and ASCE ETr methods, respectively. Median values (Fig. 8b) are similar to the average values, but the 25th and 75th percentiles and their corresponding upper whiskers (maximum values) and outliers show larger ranges in the ETr outputs. Carrillo-Rojas et al. (2016) reported average daily ETa values of 1.64 ± 0.47 mm day^{-1} to

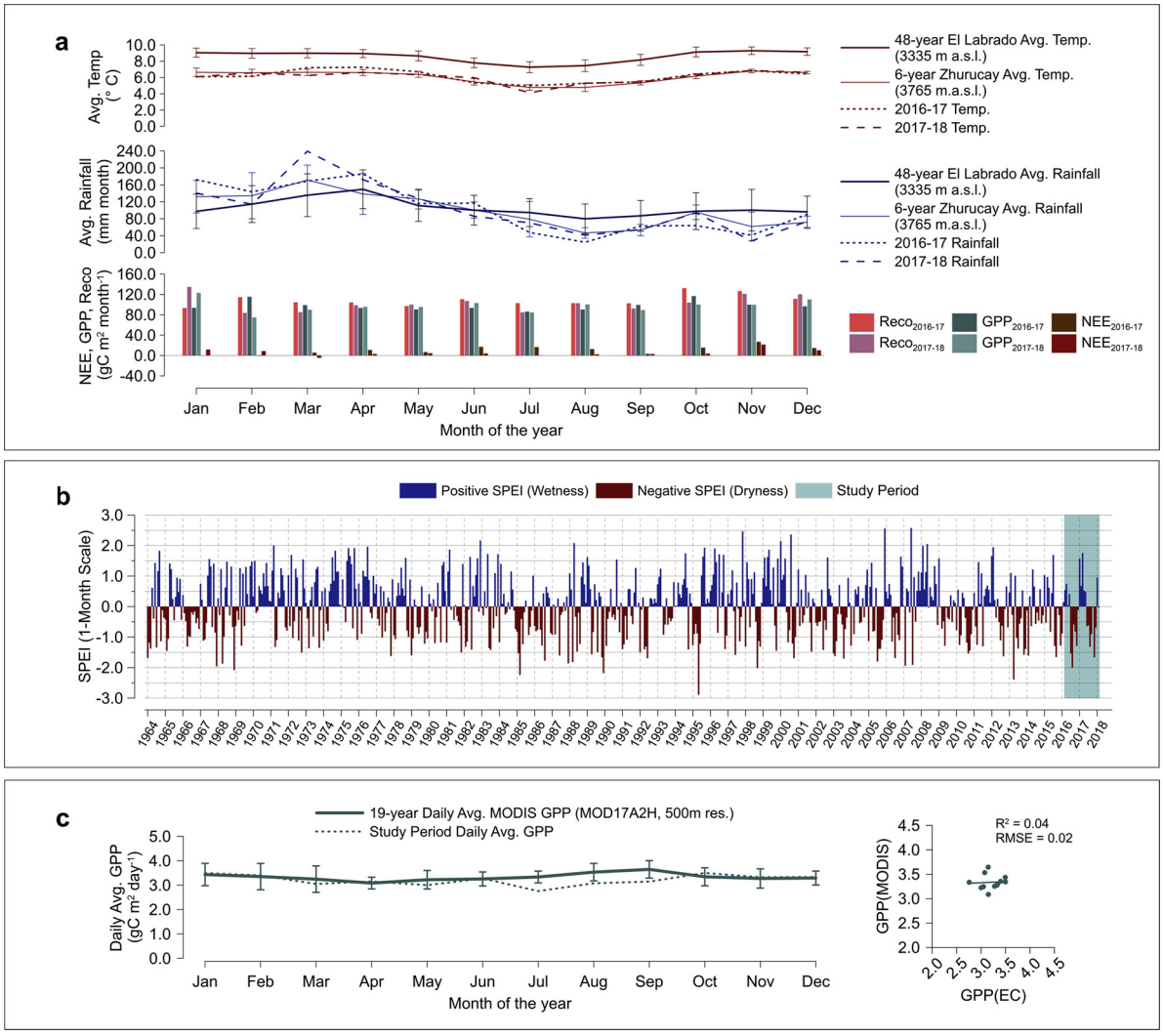

Fig. 7. Long-term analyses: (7a) Temperature and rainfall series for: El Labrado AWS, Zhurucay AWS (including the 2-year EC measurements), NEE, GPP and Reco, (7b) Historical monthly SPEI, and (7c) MODIS GPP observations versus EC-based GPP estimations.

2.27 ± 0.63 mm day^{-1} (representing the wet period and less humid period, respectively) for remotely sensed ETa maps, calculated using an energy balance based model (with Landsat imagery) of a nearby páramo catchment (Quinoas-Cajas). Córdova et al. (2015) calculated daily estimates of ETr (FAO56) of 1.89 mm day^{-1} for Quinoas-Cajas and 1.98 mm day^{-1} for Zhurucay by applying similar meteorological instruments in 2011–2013. Table 5 shows the ETa and ETr daily averages and aggregated monthly and annual estimates for the full period and for wet and less humid months. The respective Kc coefficients are also shown.

For the 2-year study period, ETa had a mean of 634.7 ± 9.0 mm per year, a lower value than the ETr sums (ETr (FAO56) mean = 702.0 ± 7.8 mm per year, and ETr (ASCE) mean = 812.1 ± 19.8 mm per year). Compared to the mean annual rain depth (1237.9 ± 3.8 mm per year), ETa accounts for 51% of the precipitation. However, this estimate may not be definitive due to limitations and uncertainties in the tipping bucket technique (TB), as was demonstrated by Padrón et al. (2015) using 3 years (2011–2014) of rainfall observations in Zhurucay. The authors showed that low-resolution techniques, such as the TB (0.1 mm), can underestimate the total rainfall catch by up to 15% compared to a high-resolution optical technique, such as a laser disdrometer (0.01 mm), which detects drizzle contributions with great accuracy. Unfortunately, this instrument was not available for our study period. Mosquera et al. (2015) showed a slightly lower water balance-based ETa result (580 mm year^{-1}) and a ratio over rainfall of 44.6% for the head microcatchment (M2) of Zhurucay (the location of our eddy tower).

The differences between the observed ETa values and the ETr estimates can be mainly attributed to the characteristics of the ETr algorithms. These characteristics include: (i) the sensitivity of ETr to the climatic variables, (ii) the method of estimation of solar energy components (particularly for Rn), and (iii) other factors, such as the crop model characteristics (e.g., canopy height, aerodynamical properties, etc.) or factors related to time-aggregation (Córdova et al., 2013). Therefore, calibrating the ETr models to better fit the tussock grass physiology and páramo environment is necessary. The full period Kc (FAO56) mean = 0.90 is higher than those values reported by (i) Buytaert et al. (2006c) (Kc = 0.42), based on an intra-annual water balance of a small Ecuadorian páramo catchment (Huagrauma) and by (ii) Iñiguez et al. (2016) (Kc = 0.67), based on a model simulation of a nearby páramo grassland area (Calluancay). The full period Kc (ASCE) mean = 0.78 is slightly lower than those reported by Carrillo-Rojas et al. (2016) in the form of the Reference Evapotranspiration Fraction ETrf (ASCE ETr Kc equivalent) for tussock grasslands of the Quinoas-Cajas (ETrf = 0.86 from Landsat-based ET mapping). Therefore, the ETr (FAO56) method and its Kc can be used for the prediction of ETa values in ecosystem analyses and water management applications.

The monthly water balance (the difference between P and ETa), as

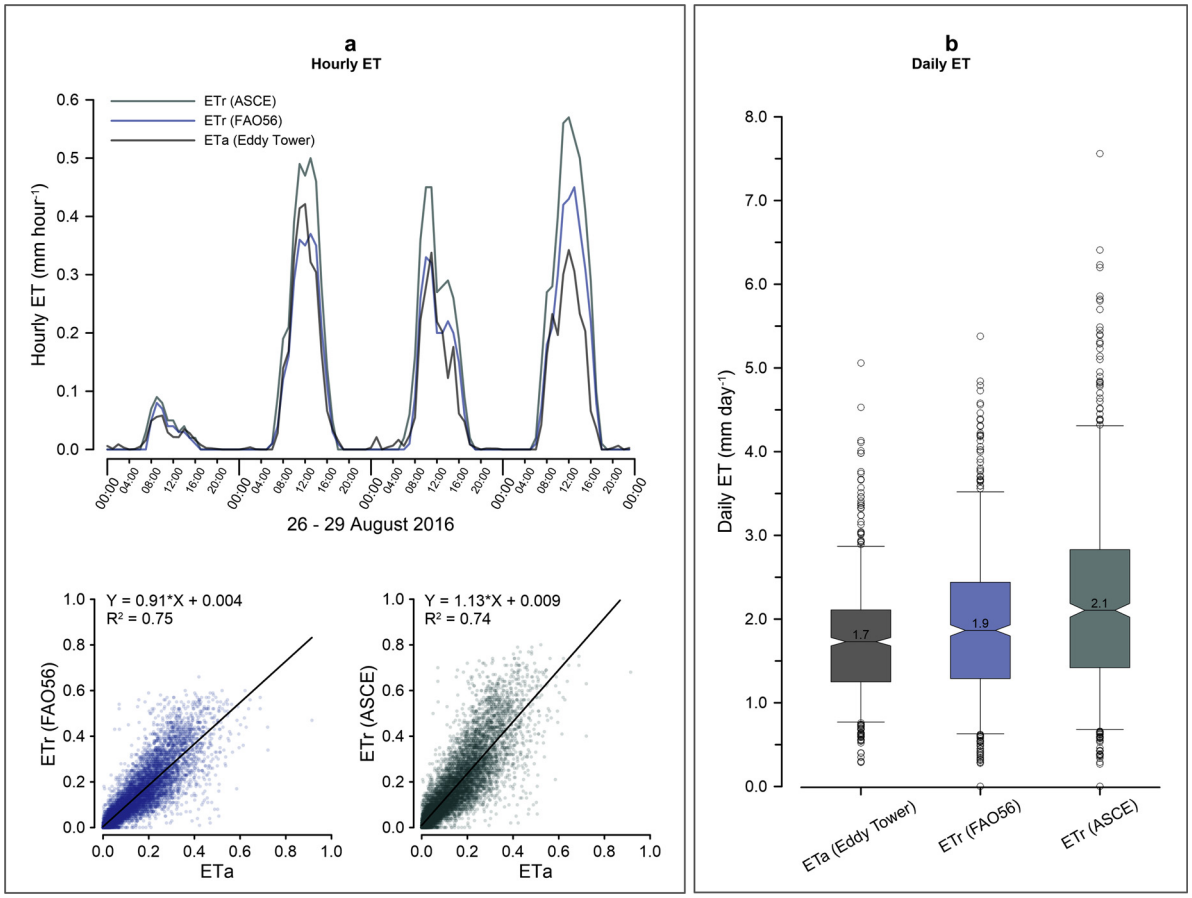

Fig. 8. Comparison of hourly ETa and ETr based on scatterplots with linear fitting and an example of ET curves for 4 days in August 2016 (8a) and of daily ET notched boxplots (95% confidence interval) (8b).

Table 5
Daily, monthly and annual ET estimates with standard deviations, and crop coefficients (Kc) for the FAO56 and ASCE ETr models.

	ETa (Eddy Tower)	ETr (FAO56)	ETr (ASCE)	Kc (FAO56)	Kc (ASCE)
Daily ET Average (mm day^{-1})	1.74 ± 0.28	1.93 ± 0.42	2.23 ± 0.49	0.90	0.78
Wet Period Daily Avg. *	1.73 ± 0.26	1.86 ± 0.56	2.12 ± 0.37	0.93	0.82
Less humid Period Daily Avg. **	1.75 ± 0.31	2.01 ± 0.51	2.37 ± 0.59	0.87	0.74
Difference Wet vs. Less humid (%)	1.3%	8.0%	12.1%		
Monthly ET Average (mm month^{-1})	52.89 ± 8.48	58.50 ± 12.72	67.67 ± 15.08	0.90	0.78
Wet Period Monthly Avg. *	52.41 ± 8.17	56.40 ± 10.26	64.18 ± 11.87	0.93	0.82
Less humid Period Monthly Avg. **	53.57 ± 8.85	61.45 ± 15.04	72.57 ± 17.53	0.87	0.74
Difference Wet vs. Less humid (%)	2.2%	9.0%	13.1%		
First Year Aggregated ET (mm year^{-1})	643.69	709.76	831.80	0.91	0.77
Second Year Aggregated ET (mm year^{-1})	625.68	694.23	792.36	0.90	0.79

* Wet period considered: January, February, March, April, May, June and October.
** Less humid period considered: July, August, September, November and December.

well as monthly rainfall and ETa, are presented in Fig. 9.

As expected, during the wet months of January, February, March, April, and May of the complete period of analysis we found a stronger positive balance (i.e., a surplus of water from the precipitation income). Surprisingly, however, for October 2016 (normally a rainy month, 6-year avg. = 95.3 mm month^{-1}), the balance result was negative (–8.8 mm month^{-1}). The latter can be attributed to the presence of short and heavy showers with considerable solar radiation in between, in contrast to other years that had consistent stratiform rainfall and an increment of cloudiness. For the months of August and November, a water deficit is clearly evident. These findings aid our understanding of potential water limitations and their occurrence in the páramo.

Finally, a review of the daily and annual ETa values retrieved from similar high-elevation (alpine) grasslands around the globe is illustrated in Table 6.

An analysis of Table 6 shows that Tibetan alpine meadows have ETa/Rain ratios of between 0.60 and 0.70 and that the North American alpine tundra has a ratio of 0.58, all three of which are higher than that of our study area (0.51). Therefore, the humid páramo experienced a diminished loss of water by evaporative processes. This is corroborated

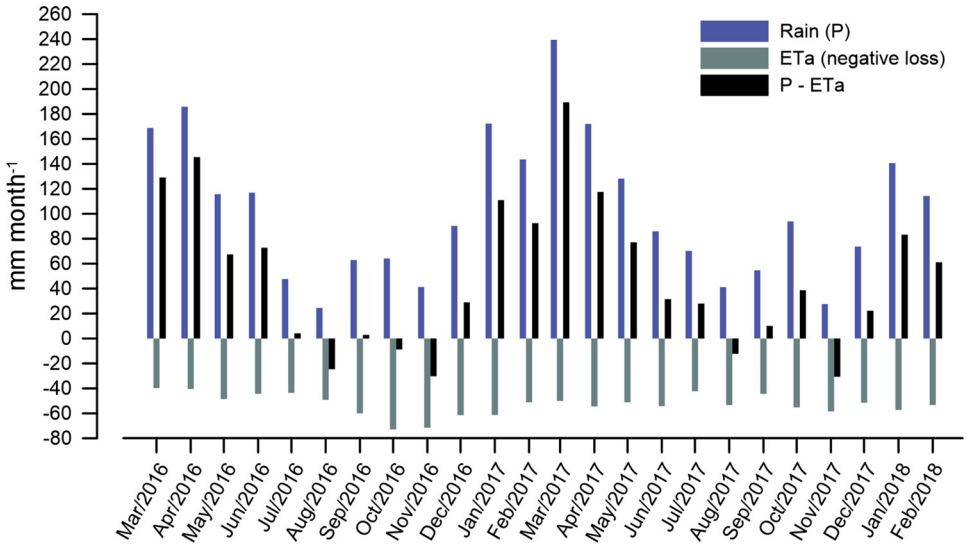

Fig. 9. Water Balance (P-ETa) at monthly scales.

by lower levels of daily ETa loss in our study area relative to those from other locations. Figure S7 in the supplementary material depicts ETa, rainfall, vapor pressure deficit (VPD) and Rn daily time series for the study period.

4. Concluding remarks

Knowledge gaps pertaining to CO_2 exchange, ETa processes and their interactions with microclimates of tropical high mountain grasslands motivated us to install the first EC tower in the highest vegetated frontier of the tropics: the Andean páramo. Our investigation provides insight into carbon / water flux behaviors at different time scales and under different climatic conditions.

The identified CO_2 budget shows that ecosystem respiration levels exceed productivity levels most of the time (66%); this outcome, in an annual balance, doubtlessly renders the Zhurucay páramo a C source. However, a long observational period is needed in future investigations to confirm the hypothesis that this location (and other páramo sites) mostly act as C sources under current climatic conditions and to understand their intra- and interannual sink / source strength. The C balance found is mainly controlled by low levels of solar energy (which limits the photosynthesis of the available biomass), via climatic controls such as low temperatures and high soil moisture and by the elevated diurnal and nocturnal respiration rates. The CO_2 light and temperature-response equations parameterized in this study will contribute to future studies on páramo EC-ungauged sites. However, the accuracy of these equations would benefit from a parameterization based on long-term data. The páramo showed limitations of C sequestration analogous to those of other high-elevation (alpine grasslands) and high-latitude (tundra) sites. However, some investigations exclusively based on soil or plant-level observations and shorter-term monitoring have suggested that this ecosystem is a CO_2 sink (Bremer et al., 2016; Farley et al., 2013; McKnight et al., 2017; Minaya et al., 2016).

Tonneijck et al. (2010) demonstrated that the C content of the páramo soils is exceptional (87 ± 12 kgC m^{-2}, up to 200 cm depth), especially in the ectorganic horizon (31 ± 23 kgC m^{-2}). If we consider a hypothetical steady loss of 0.099 kgC m^{-2} per year (our mean annual NEE), the ectorganic-layer C stock in Zhurucay would be depleted in 313 ± 232 years. Such a hypothetical situation could be worsened in climate change scenarios in which SOM degradation increases due to temperature increases (microorganism-activity acceleration) and rainfall levels diminish (soil drying) (Buytaert et al., 2011), and in which the CO_2 fertilization effect (industrial-era) could be reduced due to extreme weather conditions, as suggested by Obermeier et al. (2017) for temperate C3 grasses. In the páramo, land use / cover-change scenarios can affect the water retention capacities of soil (e.g., increasing

Table 6
Annual and daily ETa comparisons among alpine grasslands around the globe.

Location (Country)	Elev. (m a.s.l.)	Lat./ Long	Type	Rain (mm $year^{-1}$)	Annual ET (mm $year^{-1}$)	Daily ET (mm day^{-1})	ET Method *	Reference
Tibetan Kobresia pastures (China)	4410	31.26 N / 92.1 E	Alpine Meadow	430	300	1.90[a] 4.00 ~ 6.00[b]	EC, LYS, MOD	(Coners et al., 2016)
Zhurucay Páramo (Ecuador)	3765	3.06 S / 79.24 W	Alpine Tundra	1238	635	1.74	EC	(Present study)
Niwot Ridge (USA)	3500	40.05 N / 105.58 W	Alpine Tundra	1072	631	–	EC	(Knowles et al., 2015b)
Qinghai-Tibetan Plateau (China)	3250	37.58 N / 101.33 E	Alpine Meadow	642**	391**	1.90 ~ 2.22[c]	EC	(Gu et al., 2008)
Swiss Central Alps (Switzerland)	2440	46.56 N / 8.41 E	Alpine Grassland	1900	–	3.70	AT, LYS	(van den Bergh et al., 2013)

a, b: Respective values for dry and humid summer in the Tibetan Kobresia pastures.
c: Values for the growing season in the Qinghai-Tibetan Plateau.
* ET Method: EC = Eddy Covariance, LYS = Lysimeter; AT = Atmometer evaporation, MOD = Model Based.
** Averaged during 2002–2004 for the Qinghai-Tibetan Plateau site.

ET losses and water transit time) (Crespo et al., 2010; Mosquera et al., 2016b) but can also alter C dynamics and lead to irreversible changes in the hydrophilic characteristics of Andosols (favored by drying effects) (Poulenard et al., 2003). For instance, a detailed examination of the effects of climate change in the northern tropical Andes highlands by Vuille et al. (2018) projected severe shrinkages of glaciers and negative impacts on water supplies for the lowlands. Hence, a deeper understanding of effects of global-warming on large subnival ecosystems such as the páramo is also required.

To our knowledge, we present the first ETa and crop coefficients for Andean tussock grasslands, retrieved from a reliable H_2O vapor-detection technique and two widely used ETr models. These indicators are highly sought after in research on climate change, ecosystem services and water management in the Inter-Andean valleys (Célleri and Feyen, 2009; Hamel et al., 2017) and will help the scientific community and stakeholders to consider near-real losses from evaporative processes in water balances in this fragile ecosystem. Our study introduces novel and relevant data on land-atmosphere exchange processes in the high tropics, similar to other pioneering investigations of torrid-zone mountains (Cullen et al., 2007; Holwerda et al., 2006; Ibrom et al., 2008; Litt et al., 2015). The preservation of the pristine vegetation, soil and hydrology of the Andean páramo is crucial for preventing major losses in C storage and water, which have irreversible consequences for the páramo's ecosystem services.

Future works should pursue (i) the long-term EC monitoring of carbon / water fluxes to analyze interactions between drought and extremely humid periods at interannual time scales; (ii) the evaluation and improved parameterization of C light-response equations and Kc reported here, based on long-term flux datasets, (iii) the prediction of C, energy and water fluxes based on land surface–atmosphere models at landscape and regional scales, with a specific calibration of their soil and vegetation parameters; and (vi) the characterization of the effects of similar greenhouse gases, such as methane, which can be highly abundant in these soils and wetlands.

Conflicts of interest

The authors declare no conflict of interest.

Acknowledgements

This work was funded by the Research Office of the University of Cuenca (DIUC) through the Project XIII–Conc: "Estudio Comparativo de Métodos de Estimación de Evapotranspiración Actual en Suelos Húmedos de una Micro cuenca de Páramo Andino," and by the Ecuadorian Secretary of Higher Education, Science, Technology and Innovation (SENESCYT) through "Programa de Fortalecimiento de las Capacidades en Ciencia, Tecnología, Investigación e Innovación de las Instituciones de Educación Superior Públicas (2013–2014)." We thank these institutions for providing generous funding. The first author especially thanks SENESCYT and the Ecuadorian Government for funding his doctoral scholarship. We thank the German Research Foundation (DFG) and PAK823–825 "Platform for Biodiversity and Ecosystem Monitoring and Research in South Ecuador" Subproject C6 (BE1780/38–1), which supported the study in human and scientific capacities. We also thank Comuna Chumblín Sombrederas (Azuay, San Fernando) for providing logistical support, and the National Institute of Meteorology and Hydrology of Ecuador (INAMHI) for providing the El Labrado long-term dataset. We are grateful to Johanna Orellana for her valuable support of the computational implementation; to Mario Córdova, Patricio Crespo, Paul Muñoz, Olmedo Pauta, Ana Ochoa, Santiago González, Alex Avilés, Lenin Campozano and Wilson Reinoso; and to Juan Pablo Córdova for his professional support in the graphical abstract design. Finally, we thank the editor Prof. Dr. Tim J. Griffis and two anonymous reviewers for their valuable criticism and constructive comments.

Appendix A. Supplementary data

Supplementary material related to this article can be found, in the online version, at doi:https://doi.org/10.1016/j.agrformet.2018.11.006.

The aforementioned complementary illustrations (Figures S1 to S7) and Annex S1 to S3 can be found in the supplementary material.

Carbon, water, energy and micrometeorological data used in the present study will soon be available on the FLUXNET database (Site EC-APr): https://daac.ornl.gov/cgi-bin/dataset_lister.pl?p=9

References

Allen, R.G., Pereira, L.S.L., Raes, D., Smith, M., et al., 1998. Crop Evapotranspiration-guidelines for Computing Crop Water requirements-FAO Irrigation and Drainage Paper 56. FAO, Rome 300, D05109.

Aparecido, L.M.T., Teodoro, G.S., Mosquera, G., Brum, M., Barros, F., de, V., Pompeu, P.V., Rodas, M., Lazo, P., Müller, C.S., Mulligan, M., Asbjornsen, H., Moore, G.W., Oliveira, R.S., 2018. Ecohydrological drivers of Neotropical vegetation in montane ecosystems. Ecohydrology, e1932. https://doi.org/10.1002/eco.1932.

ASCE-ERWI, 2001. ASCE's Standardized Reference Evapotranspiration Equation, in: Watershed Management and Operations Management 2000. American Society of Civil Engineers, Reston, VA, pp. 1–11. https://doi.org/10.1061/40499(2000)126.

Aubinet, M., Vesala, T., Papale, D., 2012. Eddy Covariance: A Practical Guide to Measurement and Data Analysis. Springer, Netherlands, Dordrecht. https://doi.org/10.1007/978-94-007-2351-1.

Aucapiña, G., Marín, F., 2014. Efectos de la posición fisiográfica en las propiedades hidrofísicas de los suelos de páramo de la microcuenca del río Zhurucay. Grad. Thesis. Universidad de Cuenca, Ecuador.

Baldocchi, D., Chu, H., Reichstein, M., 2018. Inter-annual variability of net and gross ecosystem carbon fluxes: a review. Agric. For. Meteorol. 249, 520–533. https://doi.org/10.1016/j.agrformet.2017.05.015.

Baldocchi, D., Falge, E., Gu, L., Olson, R., Hollinger, D., Running, S., Anthoni, P., Bernhofer, C., Davis, K., Evans, R., Fuentes, J., Goldstein, A., Katul, G., Law, B., Lee, X., Malhi, Y., Meyers, T., Munger, W., Oechel, W., Paw, K.T., Pilegaard, K., Schmid, H.P., Valentini, R., Verma, S., Vesala, T., Wilson, K., Wofsy, S., 2001. FLUXNET: a new tool to study the temporal and spatial variability of ecosystem–scale carbon dioxide, water vapor, and energy flux densities. Bull. Am. Meteorol. Soc. 82, 2415–2434. https://doi.org/10.1175/1520-0477(2001)082<2415:FANTTS>2.3.CO;2.

Baldocchi, D.D., 2003. Assessing the eddy covariance technique for evaluating carbon dioxide exchange rates of ecosystems: past, present and future. Glob. Chang. Biol. 9, 479–492. https://doi.org/10.1046/j.1365-2486.2003.00629.x.

Beer, C., Reichstein, M., Tomelleri, E., Ciais, P., Jung, M., Carvalhais, N., Rodenbeck, C., Arain, M.A., Baldocchi, D., Bonan, G.B., Bondeau, A., Cescatti, A., Lasslop, G., Lindroth, A., Lomas, M., Luyssaert, S., Margolis, H., Oleson, K.W., Roupsard, O., Veenendaal, E., Viovy, N., Williams, C., Woodward, F.I., Papale, D., 2010. Terrestrial gross carbon dioxide uptake: global distribution and covariation with climate. Science (80-.) 329, 834–838. https://doi.org/10.1126/science.1184984.

Beguería, S., Vicente-Serrano, S.M., Reig, F., Latorre, B., 2014. Standardized precipitation evapotranspiration index (SPEI) revisited: parameter fitting, evapotranspiration models, tools, datasets and drought monitoring. Int. J. Climatol. 34, 3001–3023. https://doi.org/10.1002/joc.3887.

Beltrán, K., Salgado, S., Cuesta, F., León-Yánez, S., Romoleroux, K., Ortiz, E., Cardenas, A., Velástegui, A., 2009. Distribución espacial, sistemas ecológicos y caracterización florística de los páramos en el Ecuador. EcoCiencia 72–150.

Bendix, J., Rollenbeck, R., Göttlicher, D., Cermak, J., 2006. Cloud occurrence and cloud properties in Ecuador. Clim. Chang. Res. Lett. 30, 133–147. https://doi.org/10.3354/cr030133.

Bendix, J., Rollenbeck, R., Ritcher, M., Fabian, P., Emck, P., 2008. Climate. In: Beck, E., Bendix, J., Kottke, I., Makeschin, F., Mosandl, R. (Eds.), Gradients in a Tropical Mountain Ecosystem of Ecuador. Ecological Studies. Springer Verlag, Berlin, Germany, pp. 63–74.

Beringer, J., Hutley, L.B., McHugh, I., Arndt, S.K., Campbell, D., Cleugh, H.A., Cleverly, J., Resco de Dios, V., Eamus, D., Evans, B., Ewenz, C., Grace, P., Griebel, A., Haverd, V., Hinko-Najera, N., Huete, A., Isaac, P., Kanniah, K., Leuning, R., Liddell, M.J., Macfarlane, C., Meyer, W., Moore, C., Pendall, E., Phillips, A., Phillips, R.L., Prober, S.M., Restrepo-Coupe, N., Rutledge, S., Schroder, I., Silberstein, R., Southall, P., Yee, M.S., Tapper, N.J., van Gorsel, E., Vote, C., Walker, J., Wardlaw, T., 2016. An introduction to the Australian and New Zealand flux tower network – OzFlux. Biogeosciences 13, 5895–5916. https://doi.org/10.5194/bg-13-5895-2016.

Bertzky, M., Ravilious, C., Araujo Navas, A.L., Kapos, V., Carrión, D., Chíu, M., Dickson, B., 2010. Carbon, Biodiversity and Ecosystem Services: Exploring Co-benefits Ecuador. UNEP-WCMC, Cambridge, UK.

Bremer, L.L., Farley, K.A., Chadwick, O.A., Harden, C.P., 2016. Changes in carbon storage with land management promoted by payment for ecosystem services. Environ. Conserv. 43, 397–406. https://doi.org/10.1017/S0376892916000199.

Burba, G., 2013. Eddy Covariance Method-for Scientific, Industrial, Agricultural, and Regulatory Applications, Book. LI-COR Biosciences, Lincoln, Nebraska, USA. https://doi.org/10.1007/s00704-004-0095-y.

Buytaert, W., Célleri, R., De Bièvre, B., Cisneros, F., Wyseure, G., Deckers, J., Hofstede, R., 2006a. Human impact on the hydrology of the Andean páramos. Earth-Sci. Rev. 79,

53–72. https://doi.org/10.1016/j.earscirev.2006.06.002.
Buytaert, W., Cuesta-Camacho, F., Tobón, C., 2011. Potential impacts of climate change on the environmental services of humid tropical alpine regions. Glob. Ecol. Biogeogr. 20, 19–33. https://doi.org/10.1111/j.1466-8238.2010.00585.x.
Buytaert, W., Deckers, J., Wyseure, G., 2006b. Description and classification of non-allophanic Andosols in south Ecuadorian alpine grasslands (páramo). Geomorphology 73, 207–221. https://doi.org/10.1016/j.geomorph.2005.06.012.
Buytaert, W., Iñiguez, V., Célleri, R., De Bièvre, B., Wyseure, G., Deckers, J., 2006c. Analysis of the water balance of small páramo catchments in south Ecuador. Environmental Role of Wetlands in Headwaters. Springer, pp. 271–281.
Cabral, O.M.R., da Rocha, H.R., Gash, J.H., Freitas, H.C., Ligo, M.A.V., 2015. Water and energy fluxes from a woodland savanna (cerrado) in southeast Brazil. J. Hydrol. Reg. Stud. 4, 22–40. https://doi.org/10.1016/j.ejrh.2015.04.010.
Cabral, O.M.R., da Rocha, H.R., Gash, J.H., Ligo, M.A.V., Freitas, H.C., Tatsch, J.D., 2010. The energy and water balance of a Eucalyptus plantation in southeast Brazil. J. Hydrol. 388, 208–216. https://doi.org/10.1016/j.jhydrol.2010.04.041.
Carrillo-Rojas, G., Silva, B., Córdova, M., Célleri, R., Bendix, J., 2016. Dynamic mapping of evapotranspiration using an energy balance-based model over an andean páramo catchment of Southern Ecuador. Remote Sens. 8, 160. https://doi.org/10.3390/rs8020160.
Célleri, R., Feyen, J., 2009. The hydrology of tropical andean ecosystems: importance, knowledge status, and perspectives. Res. Dev. 29, 350–355. https://doi.org/10.1659/mrd.00007.
Célleri, R., Willems, P., Buytaert, W., Feyen, J., 2007. Space–time rainfall variability in the Paute basin, Ecuadorian Andes. Hydrol. Process. 21, 3316–3327. https://doi.org/10.1002/hyp.6575.
Chapin, F.S., Woodwell, G.M., Randerson, J.T., Rastetter, E.B., Lovett, G.M., Baldocchi, D.D., Clark, D.A., Harmon, M.E., Schimel, D.S., Valentini, R., Wirth, C., Aber, J.D., Cole, J.J., Goulden, M.L., Harden, J.W., Heimann, M., Howarth, R.W., Matson, P.A., McGuire, A.D., Melillo, J.M., Mooney, H.A., Neff, J.C., Houghton, R.A., Pace, M.L., Ryan, M.G., Running, S.W., Sala, O.E., Schlesinger, W.H., Schulze, E.-D., 2006. Reconciling carbon-cycle concepts, terminology, and methods. Ecosystems 9, 1041–1050. https://doi.org/10.1007/s10021-005-0105-7.
Coners, H., Babel, W., Willinghöfer, S., Biermann, T., Köhler, L., Seeber, E., Foken, T., Ma, Y., Yang, Y., Miehe, G., Leuschner, C., 2016. Evapotranspiration and water balance of high-elevation grassland on the Tibetan Plateau. J. Hydrol. 533, 557–566. https://doi.org/10.1016/j.jhydrol.2015.12.021.
Córdova, M., Carrillo-Rojas, G., Crespo, P., Wilcox, B., Célleri, R., 2015. Evaluation of the penman-monteith (FAO 56 PM) method for calculating reference evapotranspiration using limited data. Mt. Res. Dev. 35, 230–239. https://doi.org/10.1659/MRD-JOURNAL-D-14-0024.1.
Córdova, M., Carrillo, G., Célleri, R., 2013. Errores en la Estimación de la Evapotranspiración de Referencia de una zona de Páramo andino debidos al uso de datos mensuales, diarios y horarios. Aqua-LAC 5, 14–22.
Córdova, M., Célleri, R., Shellito, C.J., Orellana-Alvear, J., Abril, A., Carrillo-Rojas, G., 2016. Near-Surface Air Temperature Lapse Rate Over Complex Terrain in the Southern Ecuadorian Andes: Implications for Temperature Mapping. Arctic, Antarct. Alp. Res. 48, 678–684. https://doi.org/10.1657/AAAR0015-077.
Correa, A., Windhorst, D., Crespo, P., Célleri, R., Feyen, J., Breuer, L., 2016. Continuous versus event-based sampling: how many samples are required for deriving general hydrological understanding on Ecuador's páramo region? Hydrol. Process. 30, 4059–4073. https://doi.org/10.1002/hyp.10975.
Correa, A., Windhorst, D., Tetzlaff, D., Crespo, P., Célleri, R., Feyen, J., Breuer, L., 2017. Temporal dynamics in dominant runoff sources and flow paths in the Andean Páramo. Water Resour. Res. 53, 5998–6017. https://doi.org/10.1002/2016WR020187.
Crespo, P., Célleri, R., Buytaert, W., Feyen, J., Iñiguez, V., Borja, P., De Bièvre, B., 2010. Land use change impacts on the hydrology of wet Andean páramo ecosystems. Proceedings of the Workshop Held at Goslar-Hahnenklee 6. https://doi.org/10.13140/2.1.5137.6320.
Cuesta, F., De Bièvre, B., 2008. Páramo of Northern Andes (Venezuela, Colombia, Ecuador, northern Perú). Temperate Grasslands of South America. The World Temperate Grasslands Conservation Initiative Workshop 3–11.
Cullen, N.J., Mölg, T., Kaser, G., Steffen, K., Hardy, D.R., 2007. Energy-balance model validation on the top of Kilimanjaro, Tanzania, using eddy covariance data. Ann. Glaciol. 46, 227–233. https://doi.org/10.3189/172756407782871224.
Curiel Yuste, J., Hereş, A.-M., Ojeda, G., Paz, A., Pizano, C., García-Angulo, D., Lasso, E., 2017. Soil heterotrophic CO2 emissions from tropical high-elevation ecosystems (Páramos) and their sensitivity to temperature and moisture fluctuations. Soil Biol. Biochem. 110, 8–11. https://doi.org/10.1016/j.soilbio.2017.02.016.
Damm, A., Elbers, J.A., Erler, A., Gioli, B., Hamdi, K., Hutjes, R., Kosvancova, M., Meroni, M., Miglietta, F., Moersch, A., Moreno, J., Schickling, A., Sonnenschein, R., Udelhover, T., Van Der Linden, S., Horstet, P., Rascher, U., 2010. Remote sensing of sun-induced fluorescence to improve modeling of diurnal courses of gross primary production (GPP). Glob. Chang. Biol. 16, 171–186. https://doi.org/10.1111/j.1365-2486.2009.01908.x.
Duffie, J.A., Beckman, W.A., 2013. Solar Engineering of Thermal Processes, Second. ed, Solar Engineering of Thermal Processes, fourth edition. Wiley Interscience, New York.
Emck, P., 2007. A Climatology of South Ecuador-with Special Focus on the Major Andean Ridge As Atlantic-pacific Climate Divide. PhD Thesis. Friedrich Alexander-Universität, Erlangen-Nürnberg, Germany.
Euskirchen, E.S., Bret-Harte, M.S., Shaver, G.R., Edgar, C.W., Romanovsky, V.E., 2017. Long-term release of carbon dioxide from Arctic Tundra ecosystems in Alaska. Ecosystems 20, 960–974. https://doi.org/10.1007/s10021-016-0085-9.
Falge, E., Baldocchi, D., Olson, R., Anthoni, P., Aubinet, M., Bernhofer, C., Burba, G., Ceulemans, R., Clement, R., Dolman, H., Granier, A., Gross, P., Grünwald, T., Hollinger, D., Jensen, N.-O., Katul, G., Keronen, P., Kowalski, A., Lai, C.T., Law, B.E., Meyers, T., Moncrieff, J., Moors, E., Munger, J.W., Pilegaard, K., Rannik, Ü., Rebmann, C., Suyker, A., Tenhunen, J., Tu, K., Verma, S., Vesala, T., Wilson, K., Wofsy, S., 2001. Gap filling strategies for defensible annual sums of net ecosystem exchange. Agric. For. Meteorol. 107, 43–69. https://doi.org/10.1016/S0168-1923(00)00225-2.
Falge, E., Baldocchi, D., Tenhunen, J., Aubinet, M., Bakwin, P., Berbigier, P., Bernhofer, C., Burba, G., Clement, R., Davis, K.J., Elbers, J.A., Goldstein, A.H., Grelle, A., Granier, A., Guðmundsson, J., Hollinger, D., Kowalski, A.S., Katul, G., Law, B.E., Malhi, Y., Meyers, T., Monson, R.K., Munger, J.W., Oechel, W., Paw, U.K.T., Pilegaard, K., Rannik, Ü., Rebmann, C., Suyker, A., Valentini, R., Wilson, K., Wofsy, S., 2002. Seasonality of ecosystem respiration and gross primary production as derived from FLUXNET measurements. Agric. For. Meteorol. 113, 53–74. https://doi.org/10.1016/S0168-1923(02)00102-8.
Farley, K.A., Bremer, L.L., Harden, C.P., Hartsig, J., 2013. Changes in carbon storage under alternative land uses in biodiverse Andean grasslands: implications for payment for ecosystem services. Conserv. Lett. 6, 21–27. https://doi.org/10.1111/j.1755-263X.2012.00267.x.
Farley, K.A., Kelly, E.F., Hofstede, R.G.M., 2004. Soil organic carbon and water retention after conversion of grasslands to pine plantations in the ecuadorian Andes. Ecosystems 7, 729–739. https://doi.org/10.1007/s10021-004-0047-5.
Finkelstein, P.L., Sims, P.F., 2001. Sampling error in eddy correlation flux measurements. J. Geophys. Res. Atmos. 106, 3503–3509. https://doi.org/10.1029/2000JD900731.
Fisher, J.B., Malhi, Y., Bonal, D., Da Rocha, H.R., De Araujo, A.C., Gamo, M., Goulden, M.L., Hirano, T., Huete, A.R., Kondo, H., Kumagai, T., Loescher, H.W., Miller, S., Nobre, A.D., Nouvellon, Y., Oberbauer, S.F., Panuthai, S., Roupsard, O., Saleska, S., Tanaka, K., Tanaka, N., Tu, K.P., Von Randow, C., 2009. The land–atmosphere water flux in the tropics. Glob. Chang. Biol. 15, 2694–2714. https://doi.org/10.1111/j.1365-2486.2008.01813.x.
Foken, T., 2008. The energy balance closure problem: an overview. Ecol. Appl. 18, 1351–1367. https://doi.org/10.1890/06-0922.1.
Fratini, G., Ibrom, A., Arriga, N., Burba, G., Papale, D., 2012. Relative humidity effects on water vapour fluxes measured with closed-path eddy-covariance systems with short sampling lines. Agric. For. Meteorol. 165, 53–63. https://doi.org/10.1016/j.agrformet.2012.05.018.
Galvagno, M., Wohlfahrt, G., Cremonese, E., Filippa, G., Migliavacca, M., Mora di Cella, U., van Gorsel, E., 2017. Contribution of advection to nighttime ecosystem respiration at a mountain grassland in complex terrain. Agric. For. Meteorol. 237–238, 270–281. https://doi.org/10.1016/j.agrformet.2017.02.018.
Google Earth Pro, 2016. (November 29, 2013) Zhurucay Landscape. 3° 03' 45.50"S, 79° 14' 01.49"W, Eye Alt. 1.07km. CNES / Astrium 2016, Google Earth Pro V7.1.7.2606 (Accessed January 1 2016). .
Grace, J., Jose, J.S., Meir, P., Miranda, H.S., Montes, R.A., 2006. Productivity and carbon fluxes of tropical savannas. J. Biogeogr. 33, 387–400. https://doi.org/10.1111/j.1365-2699.2005.01448.x.
Gu, S., Tang, Y., Cui, X., Du, M., Zhao, L., Li, Y., Xu, S., Zhou, H., Kato, T., Qi, P., Zhao, X., 2008. Characterizing evapotranspiration over a meadow ecosystem on the Qinghai-Tibetan Plateau. J. Geophys. Res. 113, D08118. https://doi.org/10.1029/2007JD009173.
Hamel, P., Riveros-Iregui, D., Ballari, D., Browning, T., Célleri, R., Chandler, D., Chun, K.P., Destouni, G., Jacobs, S., Jasechko, S., Johnson, M., Krishnaswamy, J., Poca, M., Pompeu, P.V., Rocha, H., 2017. Watershed services in the humid tropics: opportunities from recent advances in ecohydrology. Ecohydrology e1921. https://doi.org/10.1002/eco.1921.
Hammerle, A., Haslwanter, A., Schmitt, M., Bahn, M., Tappeiner, U., Cernusca, A., Wohlfahrt, G., 2007. Eddy covariance measurements of carbon dioxide, latent and sensible energy fluxes above a meadow on a mountain slope. Boundary-Layer Meteorol. 122, 397–416. https://doi.org/10.1007/s10546-006-9109-x.
Harden, C.P., Hartsig, J., Farley, K.A., Lee, J., Bremer, L.L., 2013. Effects of land-use change on water in Andean Páramo Grassland soils. Ann. Assoc. Am. Geogr. 103, 375–384. https://doi.org/10.1080/00045608.2013.754655.
Heinsch, F.A., Zhao, Maosheng, Running, S.W., Kimball, J.S., Nemani, R.R., Davis, K.J., Bolstad, P.V., Cook, B.D., Desai, A.R., Ricciuto, D.M., Law, B.E., Oechel, W.C., Hyojung Kwon, Hongyan, Luo, Wofsy, S.C., Dunn, A.L., Munger, J.W., Baldocchi, D.D., Xu, Liukang, Hollinger, D.Y., Richardson, A.D., Stoy, P.C., Siqueira, M.B.S., Monson, R.K., Burns, S.P., Flanagan, L.B., 2006. Evaluation of remote sensing based terrestrial productivity from MODIS using regional tower eddy flux network observations. IEEE Trans. Geosci. Remote Sens. 44, 1908–1925. https://doi.org/10.1109/TGRS.2005.853936.
Helfter, C., Campbell, C., Dinsmore, K.J., Drewer, J., Coyle, M., Anderson, M., Skiba, U., Nemitz, E., Billett, M.F., Sutton, M.A., 2015. Drivers of long-term variability in CO_2 net ecosystem exchange in a temperate peatland. Biogeosciences 12, 1799–1811. https://doi.org/10.5194/bg-12-1799-2015.
Herzog, S.K., Martínez, R., Jørgensen, P.M., Tiessen, H., 2011. Climate Change and Biodiversity in the Tropical Andes. Inter-American Institute for Global Change Research (IAI) and Scientific Committee on Problems of the Environment (SCOPE) https://doi.org/10.13140/2.1.3718.4969.
Hiller, R., Zeeman, M.J., Eugster, W., 2008. Eddy-covariance flux measurements in the complex terrain of an Alpine Valley in Switzerland. Boundary-Layer Meteorol. 127, 449–467. https://doi.org/10.1007/s10546-008-9267-0.
Hofstede, R., Calles, J., López, V.V., Polanco, R., Torres, F., Ulloa, J., Vásquez, A., Cerra, M., 2014. Los páramos Andinos ¿Qué Sabemos? Estado de conocimiento sobre el impacto del cambio climático en el ecosistema páramo. UICN, Quito, Ecuador.
Hofstede, R.G.M., Chilito, E.J.P., Sandovals, E.M., 1995. Vegetative structure, microclimate, and leaf growth of a paramo tussock grass species, in undisturbed, burned

and grazed conditions. Vegetatio 119, 53–65. https://doi.org/10.1007/BF00047370.
Holwerda, F., Burkard, R., Eugster, W., Scatena, F.N., Meesters, A.G.C.A., Bruijnzeel, L.A., 2006. Estimating fog deposition at a Puerto Rican elfin cloud forest site: comparison of the water budget and eddy covariance methods. Hydrol. Process. 20, 2669–2692. https://doi.org/10.1002/hyp.6065.
Hribljan, J.A., Suárez, E., Heckman, K.A., Lilleskov, E.A., Chimner, R.A., 2016. Peatland carbon stocks and accumulation rates in the Ecuadorian páramo. Wetl. Ecol. Manag. 24, 113–127. https://doi.org/10.1007/s11273-016-9482-2.
Ibrom, A., Oltchev, A., June, T., Kreilein, H., Rakkibu, G., Ross, T., Panferov, O., Gravenhorst, G., 2008. Variation in photosynthetic light-use efficiency in a mountainous tropical rain forest in Indonesia. Tree Physiol. 28, 499–508. https://doi.org/10.1093/treephys/28.4.499.
Iñiguez, V., Morales, O., Cisneros, F., Bauwens, W., Wyseure, G., 2016. Analysis of the drought recovery of Andosols on southern Ecuadorian Andean páramos. Hydrol. Earth Syst. Sci. 20, 2421–2435. https://doi.org/10.5194/hess-20-2421-2016.
Janeau, J.L., Grellier, S., Podwojewski, P., 2015. Influence of rainfall interception by endemic plants versus short cycle crops on water infiltration in high altitude ecosystems of Ecuador. Hydrol. Res. 46, 1008–1018. https://doi.org/10.2166/nh2015.203.
Jantz, N., Behling, H., 2012. A Holocene environmental record reflecting vegetation, climate, and fire variability at the Páramo of Quimsacocha, southwestern Ecuadorian Andes. Veg. Hist. Archaeobot. 21, 169–185. https://doi.org/10.1007/s00334-011-0327-x.
Josse, C., Cuesta, F., Navarro, G., Barrena, V., Cabrera, E., Chacón-Moreno, E., Ferreira, W., Peralvo, M., Saito, J., Tovar, A., 2009. Ecosistemas de los Andes del Norte y Centro. Bolivia, Colombia, Ecuador, Perú y Venezuela, Secretaría General de la Comunidad Andina, Programa Regional ECOBONA-Intercooperation, CONDESAN-Proyecto Páramo Andino, Programa BioAndes, EcoCiencia, NatureServe. IAvH, LTA-UNALM, ICAE-ULA, CDC-UNALM, RUMBOL SRL, Lima, Perú.
Kljun, N., Calanca, P., Rotach, M.W., Schmid, H.P., 2015. A simple two-dimensional parameterisation for Flux Footprint Prediction (FFP). Geosci. Model Dev. 8, 3695–3713. https://doi.org/10.5194/gmd-8-3695-2015.
Knowles, J.F., Burns, S.P., Blanken, P.D., Monson, R.K., 2015a. Fluxes of energy, water, and carbon dioxide from mountain ecosystems at Niwot Ridge. Colorado. Plant Ecol. Divers. 8, 663–676. https://doi.org/10.1080/17550874.2014.904950.
Knowles, J.F., Harpold, A.A., Cowie, R., Zeliff, M., Barnard, H.R., Burns, S.P., Blanken, P.D., Morse, J.F., Williams, M.W., 2015b. The relative contributions of alpine and subalpine ecosystems to the water balance of a mountainous, headwater catchment. Hydrol. Process. 29, 4794–4808. https://doi.org/10.1002/hyp.10526.
Lasslop, G., Reichstein, M., Papale, D., Richardson, A.D., Arneth, A., Barr, A., Stoy, P., Wohlfahrt, G., 2010. Separation of net ecosystem exchange into assimilation and respiration using a light response curve approach: critical issues and global evaluation. Glob. Chang. Biol. 16, 187–208. https://doi.org/10.1111/j.1365-2486.2009.02041.x.
Leuning, R., van Gorsel, E., Massman, W.J., Isaac, P.R., 2012. Reflections on the surface energy imbalance problem. Agric. For. Meteorol. 156, 65–74. https://doi.org/10.1016/j.agrformet.2011.12.002.
Litt, M., Sicart, J.-E., Helgason, W.D., Wagnon, P., 2015. Turbulence characteristics in the atmospheric surface layer for different wind regimes over the tropical Zongo Glacier (Bolivia, 16°S). Boundary-Layer Meteorol. 154, 471–495. https://doi.org/10.1007/s10546-014-9975-6.
Llambí, L.D., Soto-W, A., Célleri, R., De Bièvre, B., Ochoa, B., Borja, P., 2012. Ecología, hidrología y suelos de páramos, Proyecto Páramo Andino. CONDENSAN, Ecuador.
Lloyd, J., Taylor, J.A., 1994. On the temperature dependence of soil respiration. Funct. Ecol. 8, 315. https://doi.org/10.2307/2389824.
Mauder, M., Foken, T., 2004. Documentation and Instruction Manual of the Eddy Covariance Software Package TK2. Universität Bayreuth, Abt. Mikrometeorologie, Arbeitsergebnisse 26-44, Bayreuth, Germany.
Mayocchi, C.L., Bristow, K.L., 1995. Soil surface heat flux: some general questions and comments on measurements. Agric. For. Meteorol. 75, 43–50. https://doi.org/10.1016/0168-1923(94)02198-S.
McKee, T.B., Doesken, N.J., Kleist, J., 1993. The relationship of drought frequency and duration to time scales. In: Proceedings of the 8th Conference on Applied Climatology. American Meteorological Society, USA. pp. 179–183.
McKnight, J.Y., Harden, C.P., Schaeffer, S.M., 2017. Soil CO2 flux trends with differences in soil moisture among four types of land use in an Ecuadorian páramo landscape. Phys. Geogr. 38, 51–61. https://doi.org/10.1080/02723646.2016.1256101.
Meirelles, M.L., Bracho, R., Ferreira, E.A.B., 2015. Carbon dioxide exchange in a tropical wet grassland. Wetl. Ecol. Manag. 23, 817–826. https://doi.org/10.1007/s11273-015-9421-7.
Mena-Vásconez, P., Hofstede, R., 2006. Los páramos ecuatorianos. Botánica Económica los Andes Cent. 91–109.
Metzger, S., Burba, G., Burns, S.P., Blanken, P.D., Li, J., Luo, H., Zulueta, R.C., 2016. Optimization of an enclosed gas analyzer sampling system for measuring eddy covariance fluxes of H2O and CO2. Atmos. Meas. Tech. 9, 1341–1359. https://doi.org/10.5194/amt-9-1341-2016.
Minaya, V., 2016. Ecohydrology of the Andes Páramo Region. PhD Thesis. Delft University of Technology, The Netherlands.
Minaya, V., Corzo, G., van der Kwast, J., Mynett, A.E., 2016. Simulating gross primary production and stand hydrological processes of páramo grasslands in the ecuadorian andean region using the Biome-BGC model. Soil Sci. 181, 335–346. https://doi.org/10.1097/SS.0000000000000154.
Mosquera, G.M., Célleri, R., Lazo, P.X., Viaché, K.B., Perakis, S.S., Crespo, P., 2016a. Combined use of isotopic and hydrometric data to conceptualize ecohydrological processes in a high-elevation tropical ecosystem. Hydrol. Process. 30, 2930–2947. https://doi.org/10.1002/hyp.10927.
Mosquera, G.M., Lazo, P.X., Célleri, R., Wilcox, B.P., Crespo, P., 2015. Runoff from tropical alpine grasslands increases with areal extent of wetlands. CATENA 125, 120–128. https://doi.org/10.1016/j.catena.2014.10.010.
Mosquera, G.M., Segura, C., Vaché, K.B., Windhorst, D., Breuer, L., Crespo, P., 2016b. Insights into the water mean transit time in a high-elevation tropical ecosystem. Hydrol. Earth Syst. Sci. 20, 2987–3004. https://doi.org/10.5194/hess-20-2987-2016.
Munger, J.W., Loescher, H.W., Luo, H., 2012. Measurement, tower, and site design considerations. In: Aubinet, M., Vesala, T., Papale, D. (Eds.), Eddy Covariance: A Practical Guide to Measurement and Data Analysis. Springer, Netherlands, Dordrecht, pp. 21–59. https://doi.org/10.1007/978-94-007-2351-1.
Myers, N., Mittermeier, R.A., Mittermeier, C.G., da Fonseca, G.A.B., Kent, J., 2000. Biodiversity hotspots for conservation priorities. Nature 403, 853–858. https://doi.org/10.1038/35002501.
Nagy, Z., Pintér, K., Pavelka, M., Darenová, E., Balogh, J., 2011. Carbon fluxes of surfaces vs. ecosystems: advantages of measuring eddy covariance and soil respiration simultaneously in dry grassland ecosystems. Biogeosciences 8, 2523–2534. https://doi.org/10.5194/bg-8-2523-2011.
Novick, K., Brantley, S., Miniat, C.F., Walker, J., Vose, J.M., 2014. Inferring the contribution of advection to total ecosystem scalar fluxes over a tall forest in complex terrain. Agric. For. Meteorol. 185, 1–13. https://doi.org/10.1016/j.agrformet.2013.10.010.
Obermeier, W.A., Lehnert, L.W., Kammann, C.I., Müller, C., Grünhage, L., Luterbacher, J., Erbs, M., Moser, G., Seibert, R., Yuan, N., Bendix, J., 2017. Reduced CO2 fertilization effect in temperate C3 grasslands under more extreme weather conditions. Nat. Clim. Chang. 7, 137–141. https://doi.org/10.1038/nclimate3191.
Ochoa-Sánchez, A., Crespo, P., Célleri, R., 2018. Quantification of rainfall interception in the high Andean tussock grasslands. Ecohydrology e1946. https://doi.org/10.1002/eco.1946.
Oechel, W.C., Laskowski, C.A., Burba, G., Gioli, B., Kalhori, A.A.M., 2014. Annual patterns and budget of CO 2 flux in an Arctic tussock tundra ecosystem. J. Geophys. Res. Biogeosci. 119, 323–339. https://doi.org/10.1002/2013JG002431.
Olmo, F., Vida, J., Foyo, I., Castro-Diez, Y., Alados-Arboledas, L., 1999. Prediction of global irradiance on inclined surfaces from horizontal global irradiance. Energy 24, 689–704. https://doi.org/10.1016/S0360-5442(99)00025-0.
Olson, D.M., Dinerstein, E., Wikramanayake, E.D., Burgess, N.D., Powell, G.V.N., Underwood, E.C., D'amico, J.A., Itoua, I., Strand, H.E., Morrison, J.C., Loucks, C.J., Allnutt, T.F., Ricketts, T.H., Kura, Y., Lamoreux, J.F., Wettengel, W.W., Hedao, P., Kassem, K.R., 2001. Terrestrial ecoregions of the world: a new map of life on earth. Bioscience 51 (933). https://doi.org/10.1641/0006-3568(2001)051[0933:TEOTWA]2.0.CO;2.
Padrón, R.S., Wilcox, B.P., Crespo, P., Célleri, R., 2015. Rainfall in the Andean Páramo: new insights from high-resolution monitoring in Southern Ecuador. J. Hydrometeorol. 16, 985–996. https://doi.org/10.1175/JHM-D-14-0135.1.
Papale, D., Reichstein, M., Aubinet, M., Canfora, E., Bernhofer, C., Kutsch, W., Longdoz, B., Rambal, S., Valentini, R., Vesala, T., Yakir, D., 2006. Towards a standardized processing of net ecosystem exchange measured with eddy covariance technique: algorithms and uncertainty estimation. Biogeosciences 3, 571–583. https://doi.org/10.5194/bg-3-571-2006.
Pepin, N., Bradley, R.S., Diaz, H.F., Baraer, M., Caceres, E.B., Forsythe, N., Fowler, H., Greenwood, G., Hashmi, M.Z., Liu, X.D., Miller, J.R., Ning, L., Ohmura, A., Palazzi, E., Rangwala, I., Schöner, W., Severskiy, I., Shahgedanova, M., Wang, M.B., Williamson, S.N., Yang, D.Q., 2015. Elevation-dependent warming in mountain regions of the world. Nat. Clim. Chang. 5, 424–430. https://doi.org/10.1038/nclimate2563.
Poulenard, J., Podwojewski, P., Herbillon, A.J., 2003. Characteristics of non-allophanic Andisols with hydric properties from the Ecuadorian Páramos. Geoderma 117, 267–281. https://doi.org/10.1016/S0016-7061(03)00128-9.
Pullens, J.W.M., Sottocornola, M., Kiely, G., Toscano, P., Gianelle, D., 2016. Carbon fluxes of an alpine peatland in Northern Italy. Agric. For. Meteorol. 220, 69–82. https://doi.org/10.1016/j.agrformet.2016.01.012.
Quichimbo, P., Tenorio, G., Borja, P., Cárdenas, I., Crespo, P., Célleri, R., 2012. Efectos sobre las propiedades físicas y químicas de los suelos por el cambio de la cobertura vegetal y uso del suelo: Páramo de Quimsacocha al sur del Ecuador. Suelos Ecuatoriales 42 (2), 138–153.
Ramsay, P.M., Oxley, E.R.B., 2001. An assessment of aboveground net primary productivity in Andean Grasslands of Central Ecuador. Mt. Res. Dev. 21, 161–167. https://doi.org/10.1659/0276-4741(2001)021[0161:AAOANP]2.0.CO;2.
Rannik, U., Sogachev, A., Foken, T., Göckede, M., Kljun, N., Leclerc, M.Y., 2012. Footprint analysis. In: Aubinet, M., Vesala, T., Papale, D. (Eds.), Eddy Covariance: A Practical Guide to Measurement and Data Analysis. Springer, Netherlands, Dordrecht, pp. 211–253. https://doi.org/10.1007/978-94-007-2351-1.
Reichstein, M., Falge, E., Baldocchi, D., Papale, D., Aubinet, M., Berbigier, P., Bernhofer, C., Buchmann, N., Gilmanov, T., Granier, A., Grunwald, T., Havrankova, K., Ilvesniemi, H., Janous, D., Knohl, A., Laurila, T., Lohila, A., Loustau, D., Matteucci, G., Meyers, T., Miglietta, F., Ourcival, J.-M., Pumpanen, J., Rambal, S., Rotenberg, E., Sanz, M., Tenhunen, J., Seufert, G., Vaccari, F., Vesala, T., Yakir, D., Valentini, R., 2005. On the separation of net ecosystem exchange into assimilation and ecosystem respiration: review and improved algorithm. Glob. Chang. Biol. 11, 1424–1439. https://doi.org/10.1111/j.1365-2486.2005.001002.x.
Reichstein, M., Migliavacca, M., Wutzler, T., Moffat, A., 2017. REddyProc R Package Version 1.0.1 [WWW Document]. URL. Dep. Biogeochem. Integr. Max Planck Inst. (Accessed December 12 2017). http://www.bgc-jena.mpg.de/bgi/index.php/Services/REddyProcWeb.
Rollenbeck, R., Trachte, K., Bendix, J., 2016. A new class of quality controls for micrometeorological data in complex tropical environments. J. Atmos. Ocean. Technol. 33, 169–183. https://doi.org/10.1175/JTECH-D-15-0062.1.

Ruimy, A., Jarvis, P.G., Baldocchi, D.D., Saugier, B., 1995. CO2 fluxes over plant canopies and solar radiation: a review. Adv. Ecol. Res. 1–68. https://doi.org/10.1016/S0065-2504(08)60063-X.

Running, S.W., Nemani, R.R., Heinsch, F.A., Zhao, M., Reeves, M., Hashimoto, H., 2004. A continuous satellite-derived measure of global terrestrial primary production. Bioscience 54 (547). https://doi.org/10.1641/0006-3568(2004)054[0547:ACSMOG]2.0.CO;2.

Sánchez, M.E., Chimner, R.A., Hribljan, J.A., Lilleskov, E.A., Suárez, E., 2017. Carbon dioxide and methane fluxes in grazed and undisturbed mountain peatlands in the Ecuadorian Andes. Mires Peat. 19, 1–18. https://doi.org/10.19189/MaP.2017.OMB.277.

Serrano-Ortiz, P., Sánchez-Cañete, E.P., Olmo, F.J., Metzger, S., Pérez-Priego, O., Carrara, A., Alados-Arboledas, L., Kowalski, A.S., 2016. Surface-parallel sensor orientation for assessing energy balance components on mountain slopes. Boundary-Layer Meteorol. 158, 489–499. https://doi.org/10.1007/s10546-015-0099-4.

Stoy, P.C., Trowbridge, A.M., Bauerle, W.L., 2014. Controls on seasonal patterns of maximum ecosystem carbon uptake and canopy-scale photosynthetic light response: contributions from both temperature and photoperiod. Photosynth. Res. 119, 49–64. https://doi.org/10.1007/s11120-013-9799-0.

Suarez, E., Medina, G., 2001. Vegetation structure and soil properties in ecuadorian Paramo Grasslands with different histories of burning and grazing. Arctic, Antarct. Alp. Res. 33, 158. https://doi.org/10.2307/1552216.

Tonneijck, F.H., Jansen, B., Nierop, K.G.J.J., Verstraten, J.M., Sevink, J., De Lange, L., 2010. Towards understanding of carbon stocks and stabilization in volcanic ash soils in natural Andean ecosystems of northern Ecuador. Eur. J. Soil Sci. 61, 392–405. https://doi.org/10.1111/j.1365-2389.2010.01241.x.

Trachte, K., Nauss, T., Bendix, J., 2010. The impact of different terrain configurations on the formation and dynamics of katabatic flows: idealised case studies. Boundary-Layer Meteorol. 134, 307–325. https://doi.org/10.1007/s10546-009-9445-8.

UNESCO, 2013. Cajas Massif Biosphere Reserve [WWW Document]. URL. (Accessed December 24 2016). http://www.unesco.org/new/en/natural-sciences/environment/ecological-sciences/%0Abiosphere-reserves/latin-america-and-the-caribbean/ecuador/macizo-del-cajas/.

van den Bergh, T., Inauen, N., Hiltbrunner, E., Körner, C., 2013. Climate and plant cover co-determine the elevational reduction in evapotranspiration in the Swiss Alps. J. Hydrol. 500, 75–83. https://doi.org/10.1016/j.jhydrol.2013.07.013.

Vicente-Serrano, S.M., Beguería, S., López-Moreno, J.I., 2010. A multiscalar drought index sensitive to global warming: the standardized precipitation evapotranspiration index. J. Clim. 23, 1696–1718. https://doi.org/10.1175/2009JCLI2909.1.

Vickers, D., Mahrt, L., 1997. Quality control and flux sampling problems for tower and aircraft data. J. Atmos. Ocean. Technol. 14, 512–526. https://doi.org/10.1175/1520-0426(1997)014<0512:QCAFSP>2.0.CO;2.

Vickers, D., Thomas, C.K., Martin, J.G., Law, B., 2009. Self-correlation between assimilation and respiration resulting from flux partitioning of eddy-covariance CO2 fluxes. Agric. For. Meteorol. 149, 1552–1555. https://doi.org/10.1016/j.agrformet.2009.03.009.

Vuille, M., Bradley, R.S., Keimig, F., 2000. Climate variability in the Andes of Ecuador and its relation to tropical pacific and Atlantic Sea surface temperature anomalies. J. Clim. 13, 2520–2535. https://doi.org/10.1175/1520-0442(2000)013<2520:CVITAO>2.0.CO;2.

Vuille, M., Bradley, R.S., Werner, M., Keimig, F., 2003. 20th century climate change in the tropical Andes: observations and model results. Clim. Change 59, 75–99. https://doi.org/10.1023/A:1024406427519.

Vuille, M., Carey, M., Huggel, C., Buytaert, W., Rabatel, A., Jacobsen, D., Soruco, A., Villacis, M., Yarleque, C., Elison Timm, O., Condom, T., Salzmann, N., Sicart, J.-E., 2018. Rapid decline of snow and ice in the tropical Andes – impacts, uncertainties and challenges ahead. Earth-Sci. Rev. 176, 195–213. https://doi.org/10.1016/j.earscirev.2017.09.019.

Wilczak, J.M., Oncley, S.P., Stage, S.A., 2001. Sonic anemometer tilt correction algorithms. Boundary-Layer Meteorol. 99, 127–150. https://doi.org/10.1023/A:1018966204465.

Wohlfahrt, G., Hammerle, A., Niedrist, G., Scholz, K., Tomelleri, E., Zhao, P., 2016. On the energy balance closure and net radiation in complex terrain. Agric. For. Meteorol. 226–227, 37–49. https://doi.org/10.1016/j.agrformet.2016.05.012.

Wolf, S., Eugster, W., Potvin, C., Turner, B.L., Buchmann, N., 2011. Carbon sequestration potential of tropical pasture compared with afforestation in Panama. Glob. Chang. Biol. 17, 2763–2780. https://doi.org/10.1111/j.1365-2486.2011.02460.x.

World Meteorological Organization, 2012. Standardized Precipitation Index User Guide (M. Svoboda, M. Hayes and D. Wood). WMO-No. 1090, Geneva, Switzerland.

WRB-IUSS, 2014. World Reference Base for Soil Resources 2014. International Soil Classification System for Naming Soils and Creating Legends for Soil Maps, World Soil Resources Report. FAO, Rome, Italy.

Zeeman, M.J., Mauder, M., Steinbrecher, R., Heidbach, K., Eckart, E., Schmid, H.P., 2017. Reduced snow cover affects productivity of upland temperate grasslands. Agric. For. Meteorol. 232, 514–526. https://doi.org/10.1016/j.agrformet.2016.09.002.

Zhao, L., Li, J., Xu, S., Zhou, H., Li, Y., Gu, S., Zhao, X., 2009. Seasonal variations in carbon dioxide exchange in an alpine wetland meadow on the Qinghai-Tibetan Plateau. Biogeosci. Discuss. 6, 9005–9044. https://doi.org/10.5194/bgd-6-9005-2009.